PONTIFICIA UNIVERSIDAD CATOLICA DE CHILE

ESCUELA DE INGENIERIA

INFLUENCE OF AXIAL LOAD IN THE SEISMIC BEHAVIOR OF REINFORCED CONCRETE WALLS WITH NONSEISMIC DETAILING

CRISTÓBAL NICOLÁS ALARCÓN OLIVARI

Thesis submitted to the Office of Research and Graduate Studies in partial fulfillment of the requirements for the Degree of Master of Science in Engineering

Advisor:

MATÍAS ANDRÉS HUBE GINESTAR

Santiago de Chile, (August, 2013)

PONTIFICIA UNIVERSIDAD CATOLICA DE CHILE

ESCUELA DE INGENIERIA

INFLUENCE OF AXIAL LOAD IN THE SEISMIC BEHAVIOR OF REINFORCED CONCRETE WALLS WITH NONSEISMIC DETAILING

CRISTÓBAL NICOLÁS ALARCÓN OLIVARI

Members of the Committee:

MATÍAS HUBE G.

JUAN CARLOS DE LA LLERA M.

PEDRO HIDALGO O.

GUILLERMO THENOUX Z.

Thesis submitted to the Office of Research and Graduate Studies in partial fulfillment of the requirements for the Degree of Master of Science in Engineering

Santiago de Chile, (August, 2013)

Dedicado a mi papa y mamá, Alejandro

y María de los Ángeles. Gracias por todo

el cariño, los quiero mucho.

ACKNOWLEDGEMENTS

I am grateful to my advisor, Professor Matías Hube, for his knowledge, motivation and support throughout this entire project. I appreciate all the time he spent guiding me and helping me conducting this thesis but also to improve as a professional and person. I am also grateful to the following professors from Pontificia Universidad Católica de Chile who were really interested in this project and gave me helpful advice specially for the laboratory tests: Carl Lüders, Juan Carlos de la Llera, Rosita Jünemann, Hernán Santa-María, Rodrigo Jordán, Cristián Sandoval, Rafael Riddell, Diego López-García, José Luis Almazán, Esteban Sáez, Mauricio López and Christian Ledezma. Special thanks to Professor Bozidar Stojadinovic who came to Chile a couple of days and participated in one the wall tests. His expertise and advice was very valuable. I am also very thankful to the engineering students who contributed in this research: Andrés Marihuén, Roberto Manieu, Felipe Quitral, José Carlos Remesar, Juan Nicolás Rendic, Máximo Ochagavía, Fabián Riquelme, Mario Saavedra, Cristián Barrueto and Álvaro Gutiérrez.

I am thankful to the engineers and technicians from DICTUC S.A and the Laboratory of the Structural and Geotechnical Engineering Department of the University who worked hardly in performing the wall tests: Jaime Arriagada, Nicolás Tapia, Elías Peña, Alejandro Cruz, Manuel Rabello, Atilio Muñoz, Armando, Camilo, Julián, Jairo and Fabián. I would also like to thank Héctor Lizana for controlling the actuators.

I am also very thankful to the other postgraduate students at the Structural and Geotechnical Engineering Department which made it a pleasant environment to work, specially: Felipe Rubilar, Felipe Toro, Alix Becerra, Antonio Salazar, Mathias Gelb, Javier Pardo, Gislaine Pardo, Daniel González, Nicolás Zegpi, Francisco Humire, Sebastián Castro and Santiago Brunet, and also to the staff of the Department: Jenifer Flores, Josefina Uribe and Carlos Abarca.

Finally, I would like to thank my family and friends for their support for my academic pursuits. I feel very fortunate to have wonderful people around.

This research has been funded by the Chilean *Fondo Nacional de Ciencia y Tecnología*, Fondecyt, through Grant #1110377 and Fondap through Grant #15110017.

TABLE OF CONTENTS

LIST OF FIGURES

LIST OF TABLES

RESUMEN

Aproximadamente el 2% de los edificios de hormigón armado de 9 pisos o más sufrió daño serio en el terremoto de Chile de 2010. El daño observado en estos muros consistió principalmente en aplastamiento del hormigón, pandeo del refuerzo vertical y apertura del refuerzo horizontal. Este daño se atribuye al bajo confinamiento del hormigón, el detallamiento inadecuado de la armadura de borde y cargas axiales elevadas. Los objetivos de esta tesis son reproducir el daño observado y estudiar la influencia de la carga axial en el comportamiento sísmico de muros de hormigón armado sin detallamiento sísmico. Para cumplir estos objetivos, se diseñaron tres muros a escala 1:2 con características representativas de los edificios chilenos dañados. Estas características fueron obtenidas de cinco edificios que sufrieron daño en el terremoto del 2010. Los muros se ensayaron bajo ciclos de desplazamientos laterales y sujetos a diferentes razones de carga axial de 0.15, 0.25 y 0.35. El modo de falla de flexo-compresión observado en los muros dañados durante el terremoto del 2010 fue reproducido en los ensayos. Los resultados experimentales indican que la carga axial elevada tiene un efecto significativo en el comportamiento y en el modo de falla de los muros de hormigón armado; ésta gatilla una peligrosa falla frágil de aplastamiento de hormigón inmediatamente después de la pérdida de recubrimiento de la sección. Se concluye que la capacidad de desplazamiento de los muros de hormigón armado se reduce casi a la mitad cuando la razón de carga axial aumenta de 0.15 a 0.35. A pesar de que las nuevas disposiciones chilenas para el diseño de muros están destinadas a prevenir este tipo de falla, más estudios se necesitan para validar el límite de razón de carga axial de 0.35 para muros con detallamiento sísmico.

Palabras Clave: hormigón armado, carga axial, muros, comportamiento sísmico, terremoto Chile.

ABSTRACT

About 2% of reinforced concrete buildings taller than nine stories suffered serious damage during 2010 Chile Earthquake. The observed damage in reinforced concrete walls involved mostly crushing of concrete, vertical reinforcement buckling and horizontal reinforcement opening. Damage in these walls is attributed to poor concrete confinement, inadequate boundary reinforcement detailing, and high axial loads. This thesis aims to reproduce the observed damage and evaluate the influence of axial loads in the seismic behavior of reinforced concrete walls with nonseismic detailing. To achieve these objectives, three identical ½-scale wall specimens were tested. These wall specimens were designed with representative characteristics that were obtained from a survey of five buildings damaged during the 2010 Earthquake. The wall specimens were tested under equal lateral displacements cycles and subjected to different constant axial load ratios of 0.15, 0.25 and 0.35. The flexural-compressive failure mode exhibited by damaged walls during the earthquake was reproduced in these tests. The experimental results indicate that high axial load has a significant effect on the seismic performance and failure mode of reinforced concrete walls. Indeed, it triggers a dangerous brittle concrete crushing failure which occurs immediately after cover concrete spalling. It is concluded that the displacement capacity of reinforced concrete walls is reduced by almost half when the axial load ratio is increased from 0.15 to 0.35. Although new Chilean provisions for reinforced concrete wall design are intended to prevent this type of failure, more studies should be performed in order to validate the axial load ratio limit of 0.35 for walls with seismic detailing imposed in the new provisions.

Keywords: reinforced concrete, axial load, shear wall, seismic behavior, Chile earthquake.

1. INTRODUCTION

On February 27th, 2010, the central south region of Chile was struck by an M_w=8.8 earthquake, one of the strongest ever measured (EERI, 2010). This earthquake impacted 500 km of Chilean coast and over 12 million people (about 72% of the country's population) experienced a Mercalli intensity of VII or stronger. A tsunami was triggered after the earthquake, which devastated several towns near the coast. Serious damage was imparted to residential and industrial buildings, highways, railroads, ports and airports. More than 80,000 residences were destroyed and more than 100,000 had substantial damage caused by the earthquake and the tsunami. The performance of tall reinforced concrete (RC) wall buildings with 9 or more stories was acceptable; about 2% of the newer building inventory presented severe damage (Jünemann et al., 2012; Massone et al., 2012) and only one of these buildings collapsed. Damage in this type of structures was most likely attributed to poor concrete confinement, inadequate boundary reinforcement detailing, and high axial loads (Jünemann et al., 2012; Wallace et al., 2012). This research is aimed to study the third factor; how the level of axial load affects the seismic performance of RC walls.

Chile is a country located in an active subduction zone and has a significant seismic history. However, its residential buildings are designed with somehow different characteristics than other seismic countries, which make them special and relevant to study after a strong earthquake. Chilean residential buildings rely on a structural system with a large number of RC walls to resist gravity and lateral loads, which provides high stiffness (Wood, 1991). The good building performance in 1985 earthquake was attributed to this high stiffness, and it was concluded that confinement in RC walls was not needed in this type of buildings. However, after 1985 Chilean construction practice evolved, mutating these buildings into taller structures with thinner walls, which led to and increase of the axial loads in walls (Massone et al., 2012). The survey performed by Jünemann et al. (2012) indicates that most of damaged buildings in 2010 were mainly

new structures constructed after year 2000 and that high axial load was a relevant factor that may have triggered the observed damage. According to Zhang and Wang (2000), and Su and Wong (2007), high axial loads reduce the wall ductility significantly. However, these conclusions were obtained by testing RC walls with transverse boundary reinforcement, which provides concrete confinement and which was not required by Chilean design codes. During a compressive failure of a well confined RC wall, the axial strength is not reduced after cover concrete spalling; the concrete core becomes stronger due to confinement, and the plasticity is distributed along the wall height. However, if confinement is poor, damage concentrates in a reduced region of the wall causing a brittle flexural-compressive failure which is induced by crushing of concrete and buckling of vertical reinforcement bars, as was observed in some walls of damaged Chilean buildings (Figure 1.1).

Figure 1.1. Flexural-compressive failure in damaged Chilean walls

This thesis aims to reproduce the damage observed is walls during the 2010 Earthquake and to evaluate the cyclic behavior of RC walls subjected to high axial load ratios (ALRs) using an experimental campaign. The ALR is the defined as $N/f'_c A_g$, where N is the axial load, f'_c the concrete compressive strength, and Ag the gross cross section of the wall. The findings from this thesis are intended to be considered in future design provisions in Chile for RC walls in order to avoid the brittle failure mode observed in 2010.

To achieve the presented objectives, three ½-scale identical RC wall specimens were tested. These wall specimens were designed with representative characteristics of damaged buildings, which were obtained from a survey of walls from five damaged RC wall buildings. The average reinforcement ratios, wall thicknesses, ALRs and M/Vl_w ratios (where M is the moment at the base of the wall, V the shear load and l_w the wall length) were studied to design the prototype wall for conducting the experiments. The three wall specimens were tested under equal lateral cyclic displacements and subjected to different constant ALRs in order to reproduce the observed failure in RC walls. The influence of ALR in the cracking process, strength and deformation capacity of walls was studied from the observed behavior and the load-displacement relationships of the wall specimens.

The literature review of this research is given in Chapter 2 which describes the characteristics of Chilean buildings that made them susceptible to the observed damage in 2010. The ALR limits for RC walls in design codes from other countries are compared in Chapter 2 with the new ALR limit adopted in Chile, and also previous experimental research involving RC wall tests are also summarized in this Chapter. Chapter 3 describes the survey performed to five damaged RC buildings in order to obtain representative wall characteristics that were considered in the experimental campaign. Additionally, an analytical study was performed to a selected RC wall that was damaged during the 2010 Earthquake in order to explain the observed failure. The experimental program which includes the specimen design, construction, material testing, test setup, instrumentation and load application, is described in Chapter 4. A pre-test analysis in order to study the flexural behavior of the wall specimens is shown in Chapter 5. Chapter 6 shows the test results and a comparison between the behaviors of the three wall specimens is discussed in this Chapter. Finally, the analytical and experimental results are compared in Chapter 7 and conclusions obtained after this study are listed in Chapter 8, where the Chilean wall characteristics which triggered the damage and the findings from the test results are discussed.

2. BACKGROUND

The structural characteristics of Chilean RC walls for residential buildings and how they have been evolving through history is discussed in this Chapter. After the strong earthquakes of 1985 and 2010, the Chilean seismic design codes had been modified, and a limit to the axial load for RC walls was introduced in 2011. This limit is discussed in this Chapter and compared with the limit of other design codes. At the end on this Chapter, previous experiments conducted to study the seismic behavior of walls are reviewed, leading to a discussion of how high axial loads affect the seismic behavior of RC walls.

2.1 Chilean RC Shear Wall Buildings

Chilean residential buildings follow a special type of configuration called “fish-bone” (Jünemann et al., 2012). It consists on a structural system of RC walls that follow the architectural layout of the building (Figure 2.1). Each floor usually has a central longitudinal corridor with long walls and shorter transverse walls that separate apartments and rooms from each other. The transverse walls typically run from the central corridor towards the exterior of the building. Figure 2.2 and Figure 2.3 show pictures of representative Chilean residential buildings.

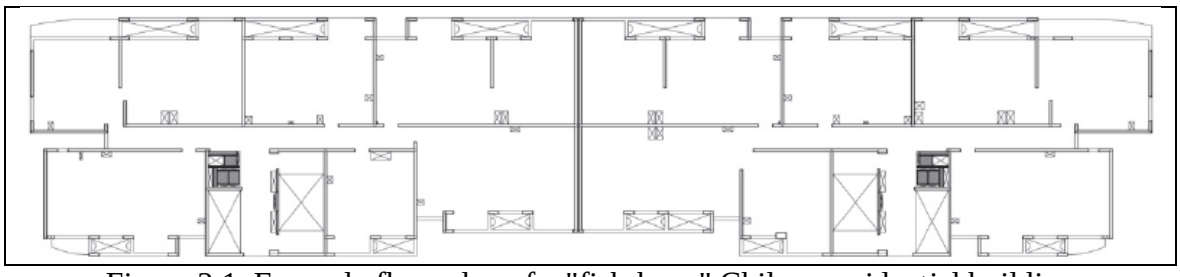

Figure 2.1. Example floor plan of a "fish-bone" Chilean residential building

Figure 2.2. Chilean residential building under construction

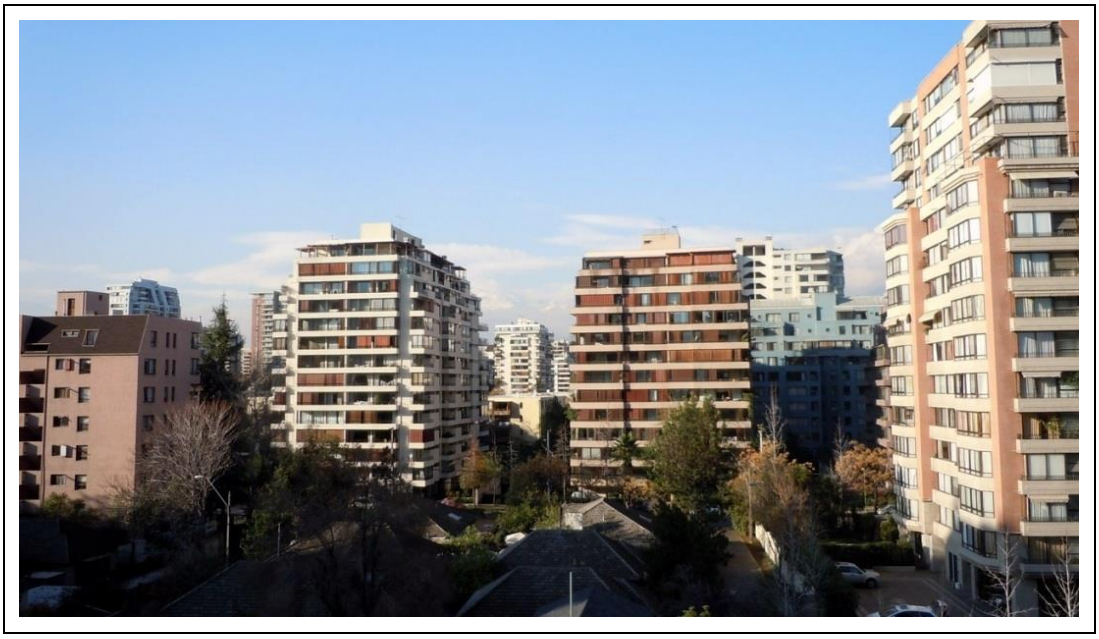

Figure 2.3. Residential buildings in Santiago, Chile

Although the Chilean seismic design philosophy with respect to acceptable damage and safety is similar to the one accepted worldwide, Chilean residential buildings are usually different than those from other countries with important seismic history like the U.S. or Japan. Most of Chilean moderate-rise residential buildings rely on a large number of RC

walls to resist gravity and lateral loads which provide high lateral stiffness for the buildings (Wood, 1991).

Chilean RC wall buildings performed extremely well during 1985 Chile Earthquake. In the city of Viña del Mar, less than 4% of the buildings suffered major damage (Riddell et al., 1987). Most of the buildings sustained no structural damage because of the large amount of wall area in each direction of the building. The ratio of wall cross sectional area to floor plan area in Chilean RC buildings is independent of their height and age, and its average ratio is about 3% in each direction of the building (Riddell et al., 1987; Jünemann et al., 2012; Massone et al., 2012). As a result of this large amount of wall area, Chilean buildings are very stiff, which explain the good performance during the 1985 earthquake even in cases where deficiencies in detailing, construction and inspection were identified (Wood et al., 1987). This satisfactory performance contradicted the philosophy in US building codes where the emphasis is on providing reinforcement confinement to ensure a ductile behavior. Wood (1991) concluded that building stiffness can eliminate the need for toughness in structural walls and reinforcement confinement might not be required at wall boundaries if drift is controlled. For building with such wall ratio, drift is likely to be in the order of 1% during a strong earthquake (Wood, 1991). Because of the lesson learned after the 1985 earthquake, the ACI 318-95 (1995) requirements for special boundary elements in RC walls were excluded in NCh433 (INN, 1996).

Chilean design and construction of buildings evolved after the 1985 earthquake. A boom in the construction that started in the 90's plus the introduction and development of computing modeling programs have influenced changes in the design. Buildings became taller and more slender, and wall thicknesses decreased (Jünemann et al., 2012; Massone et al., 2012). In many cases, buildings with 20 stories were built with 15- 20 cm wall thicknesses. These changes lead to an increase of the wall axial loads due to gravity loads. A survey of 34 damaged buildings after 2010 Chile earthquake conducted by Jünemann et al. (2012) concluded that walls of damaged RC buildings were subjected to

an average ALR of 0.10 for walls located in the first floor. The average ALR increased to 0.12 in walls of the first subterranean floor due to large vertical irregularities between the first story and the subterranean level. When earthquake loads are added, ALRs reach higher levels varying generally from 0.20 to 0.50 (Massone et al., 2012).

At the time of the 2010 earthquake the seismic design of Chilean RC buildings followed two codes: NCh433 (INN, 2009) which refers to the seismic design of structures and NCh430 (INN, 2008) which focuses on the design of RC structures. The NCh433 (INN, 1996) neglected the ACI 318-95 (1995) transverse reinforcement requirements for providing concrete confinement before the modification done in 2009. This implies that about 2000 mid-rise and high-rise RC buildings were built without special boundary elements (Wallace et al., 2012). NCh430 is based on the ACI 318-05 (2005) and the confinement provisions are not excluded in this code. Although, NCh430 lacks a limit to both wall thickness and wall axial load. After 2010 earthquake, the Chilean seismic codes where modified by decree DS 60 (2011) and decree DS 61 (2011). The first one uses ACI 318-08 (2008) as the base code but among other modifications, it imposes a limit for the ALR of walls, a criteria for the confinement of wall boundaries, and a minimum wall thickness of 30 cm for walls that require confinement.

2.2 Axial Load Limits for RC Shear Walls in Design Codes

An axial load limit for RC walls was introduced in Chilean seismic design code after the 2010 earthquake in decree DS 60 (2011). The factored ALR is limited to 0.35. In seismic design codes around the world, there are also some limitations for ALR which are summarized below.

In the Eurocode (European Comittee for Standardization, 2004), the maximum allowed ALR for primary seismic RC walls is 0.40 or 0.35 for medium ductility class or high ductility class, respectively. The ductility class depends on the hysteretic dissipation

capacity of the wall. This limit is similar than that of UBC-97 (1997), where the ALR is limited to 0.35.

In the case of the ACI 318-11 (2011), the axial strength in compression members is limited in section 10.3.6 for non prestressed member with tie reinforcement by:

$$P_{n,max} = 0.80\ \phi\ (0.85\ \mathrm{f_c'}\ (\mathrm{A_g} - \mathrm{A_{st}}) + f_y A_{st}) \quad (1)$$

Where $P_{n,max}$ is the design axial strength of the element, ϕ is the strength reduction factor for compression-controlled sections, and $\mathrm{A_{st}}$ is the vertical reinforcement area. If the strength reduction factor is not considered, and the reinforcement contribution is neglected, the maximum ALR for walls is 0.68. However, in the empirical design method proposed for rectangular RC walls in Section 14.5 of the ACI code, the axial wall strength is limited by:

$$\phi P_n = 0.55\phi f_c' A_g \left(1 - \left(\frac{k\ l_c}{32\ h}\right)^2\right) \quad (2)$$

Where P_n is the nominal axial strength of the cross section, k is the effective length factor (k = 0.8 was considered, which corresponds for a wall with restricted lateral displacement at both ends and restricted rotation at one or both ends), l_c is the wall height, and h is the wall thickness. Assuming typical dimensions of Chilean walls ($l_c =$ 2-3 m and h = 15-30 cm) and without considering the reduction factor ϕ, the maximum ALR for walls is limited to about 0.4-0.5.

The axial strength limit in Canadian design code, CSA A23.3-04 (2004), is similar than that of ACI318. Equation 14-1 of the Canadian code limits the axial strength of walls with the following equation:

$$P_r = \frac{2}{3}\alpha_1 \phi_c f_c' A_g \left(1 - \left(\frac{k h_u}{32 t}\right)^2\right) \quad (3)$$

Where P_r is the factored axial strength of the wall, α_1 is the ratio of average stress in the compression block to the specified concrete strength, ϕ_c is the strength reduction factor,

A_g is the gross area of the section, *k* is the effective length factor, h_u is the unsupported vertical height of wall between horizontal supports and *t* is the walls thickness. Similar to the ACI 318, the maximum ALR is limited to about 0.40-0.50 when typical dimensions of Chilean RC walls are taken into consideration and without considering the reduction factor ϕ_c.

In the NSZ 3101 (Standards New Zealand, 2006) the stability of walls in terms of the prevention of buckling is important in the design. Clause 11.3.7 establishes that if the design axial load at the ultimate state (N*) is larger than $0.2\ f_c'\ A_g$, wall slenderness must be controlled as:

$$(kL_n/t)\ \leq 30 \tag{4}$$

Where *k* is the effective length factor, L_n is the clear vertical distance between floors or other effective horizontal lines of lateral support, or clear span of the wall, *t* is the wall thickness.

In the Mexican code, NTCC-04 (Gobierno del Distrito Federal, 2004) if the ALR of RC walls exceeds 0.3, requirements for vertical reinforcement are more exigent and wall buckling must be restricted with lateral support.

Finally, in the Chinese Code for seismic design of buildings (China Ministry of Construction, 2010) the axial stress should not be greater than $0.50\ f_c$ for RC walls in high rise buildings located in severe seismic zones. In this code f_c is the design value of axial compressive strength of concrete, different from f_c' considered in the other codes which refers to the compressive cylinder strength of concrete. Assuming that the relation between concrete strengths is $f_c' = 0.85 f_c$, the axial stress limit in the Chinese code is equivalent to $0.59 f_c'$.

From the bibliographical study described here it can be concluded that the axial load limit adopted by the recent Chilean decree DS60 (2011) is the same that the one from Eurocode 8 for walls with high ductility and the one from UBC-97. Additionally, the

limit of DS60 (2011) is more conservative than the implicit limits established by the American and Canadian Codes. For the Mexican and the New Zealander codes, there is no axial load limit, but if the ALR is higher than the limits shown in Table 2.1, some requirements to prevent wall buckling must be satisfied.

Table 2.1. Limit of ALRs ($N/f'_c A_g$) in design codes

Decree N60 (Chile)	Eurocode 8 (Europe)	UBC-97	ACI 318-11 (USA)	CSA A23.3-04 (Canada)	NZS3101-2006 (New Zealand)	NTCC-04 (Mexico)	GB50011-2010 (China)
0.35	0.35-0.4	0.35	~ 0.4-0.5	~ 0.4-0.5	0.2*	0.3*	0.50**

*Not a limit, but if the ALR is higher the design is restricted.
** The Chinese code considers a different definition for the concrete strength.

2.3 Previous Experimental Research in the Field

The seismic behavior of RC walls had been widely studied experimentally and analytically. Walls should be designed to develop a ductile flexural behavior consistent with the structural modification factor R, and hence, brittle modes of failure should be avoided. However, the ductile flexural behavior may be affected if the wall is subjected to high compressive stresses. This section describes previous experimental research of RC walls that are relevant for this study.

Hidalgo et al. (2002) tested 26 squat walls to study the shear failure mode of Chilean RC walls. Because shear strength was the goal, these walls were tested conservatively without axial load to provide a lower bound of the shear strength, since ACI 318 (2011) neglects this effect. The walls tested had low aspect ratio with M/Vl_w ratios from 0.35 to 1.00, where M is the bending moment at the base of the wall, V is the shear load and l_w the length of the wall. It was concluded that deformation capacity of walls gets smaller as the M/Vl_w ratio decreases but the energy dissipation of walls is not affected with the variation of M/Vl_w ratio.

Takahasi et al. (2013) tested 10 specimens in order to study the flexural drift capacity of RC walls with low confinement. Their research is influenced by the damaged wall buildings after 2010 Chile Earthquake, which exhibited a brittle performance. All the wall specimens had a boundary column on only one side. The test parameters were wall length, thickness, detailing and ALR. One wall was tested without axial loads and for the other walls an ALR around 0.2 was used. The M/Vl_w ratios of the walls were between 1.26 and 2.48, the wall thicknesses between 90 and 140 mm and the wall lengths between 720 and 1800 mm. The lateral and vertical reinforcement ratios were between 0.0054 and 0.0084 and between 0.0019 and 0.0030, respectively. All the tested walls failed in compression after flexural yielding and their observed drift capacity were between 0.004 and 0.012. From the experiments, Takashi et al. proposed equations to predict the drift capacity of walls where the plastic hinge length is assumed as 2.5 times the wall thickness.

The effect of high axial loads on the behavior of RC shear walls was studied by Zhang and Wang (2000). They tested four walls designed as a prototype of a 50-story RC building located in Shanghai, China, subjected to ALRs of 0.24 and 0.35. The authors noticed that in past experiments, most walls were tested under ALRs smaller than 0.15 and they claimed that in China: "*it is not uncommon, in practice, that axial-load ratios of shear walls under design gravity load and seismic action are as high as 0.3 to 0.6*". The aspect ratio h/l_w of the wall specimens was 2.5 and the M/Vl_w ratio was 2.14. Three specimens (SW7, SW8 and SW9) were typical RC walls and the forth one (SRCW12) included a steel channel as longitudinal reinforcement. Adequate confinement was provided to prevent buckling of the longitudinal bars. The vertical and horizontal web reinforcement ratios of the four specimens were 0.0067 and 0.0101, respectively, but the ratio of main flexural reinforcement was different is each specimen: 0.0088 for SW7, 0.0065 for SW8, 0.0180 for SW9, and 0.0153 for SRCW12. Each specimen was tested under different combinations of axial load and horizontal load reversals. An ALR of 0.25 was applied to specimen SW7 and SW9, and 0.35 was applied to specimen SW8 and SRCW12. A shear compressive ratio (V_{max}/f_cA_g) of

0.106 was applied to SW7, 0.109 to SW8, 0.134 to SW9 and 0.151 to SRCW12. After performing the experiments and analyzing the results, Zhang and Wang concluded that the axial load affects the cracking pattern, the flexural strength, the failure mode, and the ductility of RC walls.

Su and Wong (2007) tested three slender RC walls subjected to ALRs of 0.25 and 0.5. They noticed that the axial load could reach high levels in medium and high rise buildings in Hong Kong. Under working conditions, the ALR in walls could be between 0.3 and 0.5. Three RC walls were fabricated with h/l_w ratios of 4. The first two specimens (W1 and W2) were detailed identical, with a longitudinal reinforcement ratio of 0.0196 and a transverse reinforcement ratio in the plastic hinge zone of 0.0054, but wall W1 was tested with an ALR of 0.25 and wall W2 with 0.5. The third wall (W3) was detailed with a longitudinal reinforcement ratio of 0.0196 and a transverse reinforcement ratio in the plastic hinge zone of 0.0108, and was tested under and ALR of 0.5. The experiments showed a ductile flexural failure in wall W1 and a brittle compressive failure in walls W2 and W3 which were subjected to high ALR. Thus, high axial load had a suppressive effect on ductility and energy dissipation of the walls.

Based on the test results of Zhang and Wang (2000) and Su and Wong (2007) it can be concluded that ALR affects the performance of RC shear walls. High axial loads reduce the ductility significantly mainly because of the brittle out-of-plane buckling mode of failure. However, in both research projects their authors concluded that more experiments are required in order to develop a rational procedure to limit the ALR in RC walls based on performance.

3. SURVEY OF DAMAGED BUILDINGS

A survey of critical walls of damaged RC buildings was conducted to obtain representative characteristics of damaged walls. These characteristics were used to define a prototype wall for conducting the experimental campaign of this research. General characteristics of five seriously damaged RC buildings and relevant properties of their walls are considered. Only rectangular walls are included in this survey because the experiments were limited to such sections. At the end on this Chapter one damaged wall is studied analytically in order to explain the damage.

3.1 Building Characteristics

Five damaged buildings (Figure 3.1) were considered in this survey in order to study the relevant characteristics of their RC walls. Four of these buildings are located in Concepción (CM, AH, PR and AA) and one in Santiago (EM). All these buildings can be considered high-rise buildings because they have between 12 and 20 stories (Table 3.1). The specified concrete strength is f_c' = 20 MPa for PR and EM buildings and f_c' = 25 MPa for CM, AH and AA buildings. The characteristics of the buildings located in Concepción were obtained from the survey performed by Westenenk et al. (2012).

Figure 3.1. Damaged buildings surveyed

Table 3.1. Number of stories of surveyed buildings

Building	CM	AH	PR	AA	EM
Number of stories + subterranean floors	18+1	15+2	13+1	20+1	20+4

3.2 Wall Characteristics

Some relevant characteristics of RC walls of the five damaged buildings are summarized in this section. The wall characteristics considered are: wall length, wall thickness, ALR, M/Vl_w ratio, and reinforcement ratios. For this purpose walls of the first two stories and the basements - where damage usually concentrated– were considered. For this survey, 27, 20, 14, 22 and 4 critical walls were considered for CM, AH, PR, AA and EM buildings respectively. Some examples of the induced damage on these walls are show in Figure 3.2. The wall thicknesses of the four buildings located in Concepción range between 15 and 20 cm and, for the EM building, the range was between 17 and 25 cm.

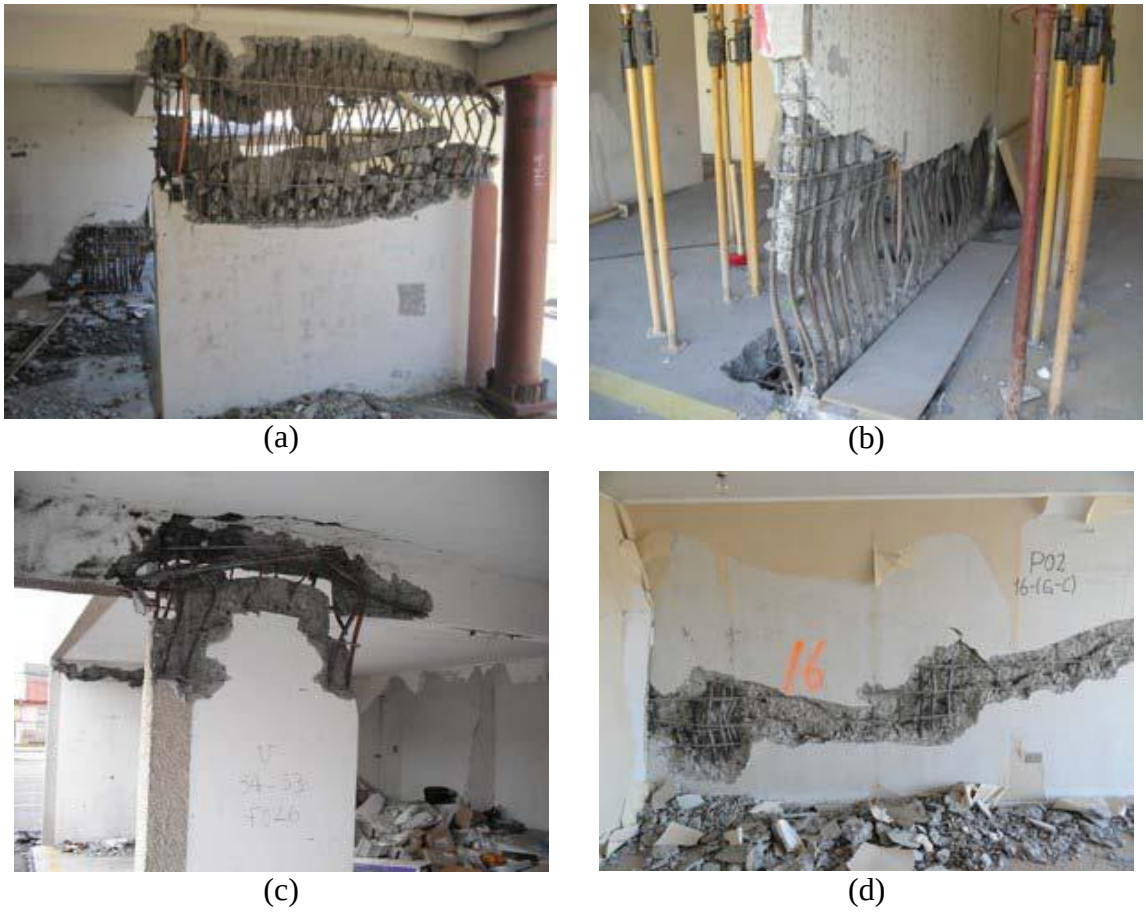

Figure 3.2. Damaged walls in (a) CM (b) AH (c) PR (d) AA buildings

The vertical loads and the M/Vl_w ratios were obtained from finite element models of the buildings using ETABS software (Computers & Structures, 2011) and following the Chilean Code NCh433 (INN, 2009). The finite element models were constructed by Westenenk et al. (2012). The M/Vl_w ratio is an important property for the behavior of walls, where *M* is the moment at the base of the wall, *V* the shear load and l_w the length of the wall. If this ratio is small the wall is considered squat and probably will exhibit a shear mode of failure (Hidalgo et al., 2002). This ratio was calculated at the base of the walls using the finite element models. The seismic load following the NCh433 (INN, 2009) was considered for the calculation of *M* and *V*. The wall length (l_w) was obtained from the structural drawings of the buildings. The average of the mean M/Vl_w ratios of the selected walls of damaged buildings is 2.02, which means that these walls are not squat, and hence, flexural behavior is relevant. The M/Vl_w ratios of walls from the damaged buildings and the average ratio are shown in Figure 3.3.

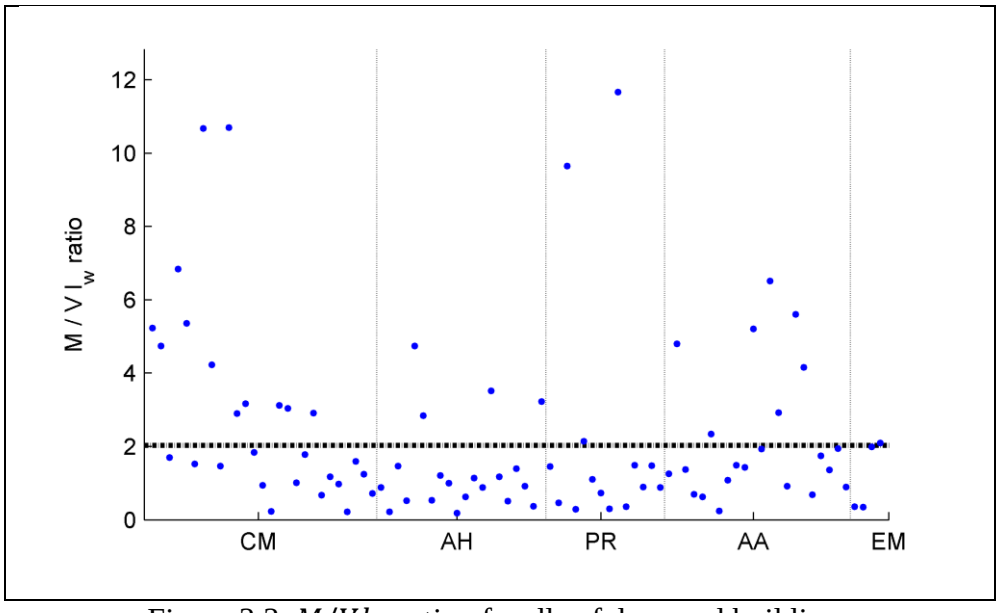

Figure 3.3. M/Vl_w ratio of walls of damaged buildings

The ALRs of the surveyed walls of the damaged buildings for gravitational load considering dead load and 25% of live load (D+0.25L) are shown in Figure 3.4. The average of the mean ALRs of walls of the five damaged buildings is 0.18. The ratios are distributed mostly between 0.1 and 0.25 in CM, AH and PR buildings. The average ALR of the walls is 0.13, 0.17, 0.13, 0.11, and 0.36, for buildings CM, AH, PR, AA, and EM, respectively.

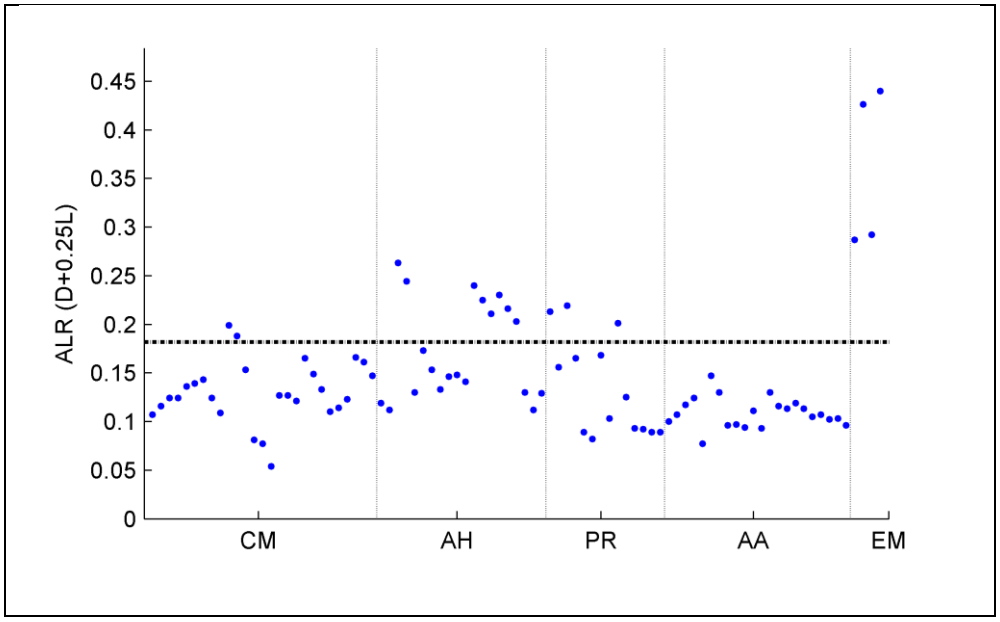

Figure 3.4. Axial load ratio due to gravity loads in walls of damaged buildings

The axial load in walls increases significantly due to the seismic overturning moment (Jünemann et al., 2012). The axial load in the walls induced by an earthquake was estimated using modal spectrum analysis according to NCh433 (INN, 2009). Figure 3.5 shows the ALRs of walls of damaged buildings under gravitational plus earthquake loads (D+0.25L+E). The average of the means of the five buildings is 0.27, which is 50% larger than that with only gravitational loads. The average ALR of the walls is 0.20, 0.28, 0.27, 0.19, and 0.42, for buildings CM, AH, PR, AA, and EM, respectively. Figure 3.5 shows that about 10% of the walls are subjected to ALRs higher than 0.35, which is the limit imposed after the 2010 Chile Earthquake (DS 60, 2011) for ultimate loads. Also, only 20% of the walls exhibit ALRs lower than 0.15 which are unlikely to trigger

compression-controlled failure modes and about 70% of the walls exhibit ALRs between 0.15 and 0.35. This range of ALRs was considered in the experimental program described later in Chapter 4. However, if the load combination 1.2D+1.0L+1.4E is considered in this analysis according to NCh3171 (INN, 2010) the average of the mean ALR of the five buildings increases to 0.38 and the percentage of walls with ALR higher than 0.35 increases to 37%.

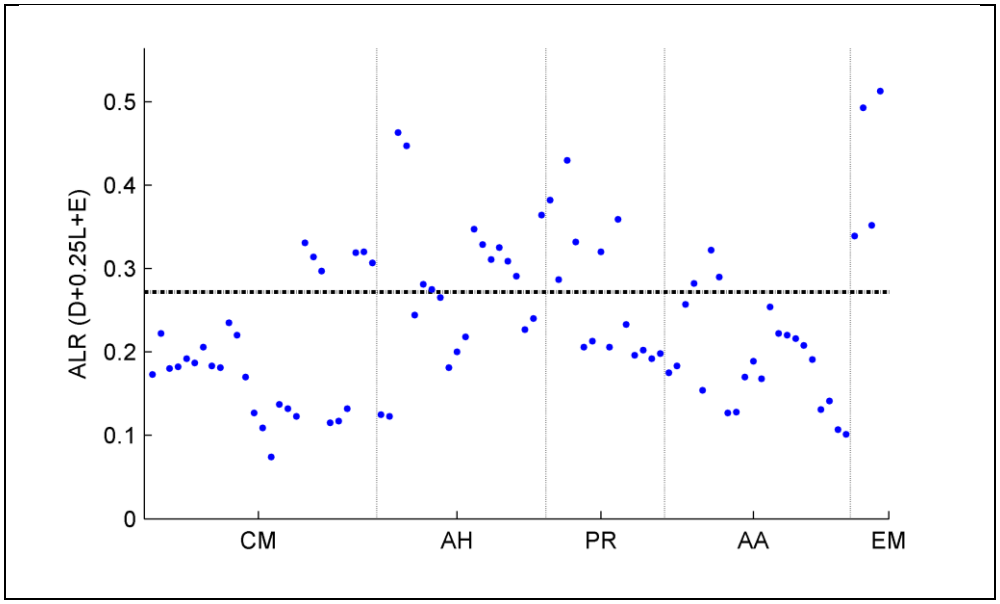

Figure 3.5. Axial load ratio due to gravity and earthquake loads in walls of damaged buildings

The comparison between the inelastic design spectrum and the elastic response spectrum from ground motions recorded near the four buildings located in Concepción is summarized in Table 3.2. The fundamental period of the buildings, soil type, the ordinate of the elastic design spectrum (Sae) at the fundamental periods, and the ordinate of the response spectrum at the fundamental period of the buildings corresponding to the closets sites with a recorded ground motion, were obtained from Westenenek et al. (2012). Table 3.2 also summarizes the strength reduction factor (R*) according to the design code and the factored inelastic design spectrum (1.4 Sae/R*). If an elastic behavior of the buildings is assumed, which is a reasonable assumption before the brittle

damage occurred in RC walls, the response spectrum ordinate is 12.0, 5.4, 2.1, and 12.1 times the factored inelastic design spectrum for buildings CM, AH, PR and AA, respectively. Therefore, the actual axial load demands in RC walls during the 2010 earthquake may be even larger than those estimated previously,

Table 3.2. Comparison between inelastic design spectrum and response spectrum for buildings located in Concepción.

Building	**Building period (sec)**	**Soil Type**	**Elastic design spectrum (m/s^2)**	**Strength reduction factor**	**Inelastic design spectrum (m/s^2)**	**Response spectrum (m/s^2)**
CM	0.80	II	4.05	8.8	0.65	7.74
AH	0.78	III	10.49	6.3	2.31	12.56
PR	0.50	III	12.11	5.2	3.29	7.06
AA	0.71	II	4.79	8.5	0.79	9.51

The vertical boundary reinforcement ratios ($\rho = A_s/l_w t_w$) of the surveyed walls of the five buildings are summarized in Table 3.3. The table includes for each building, the minimum, maximum, mean and the standard deviation of the boundary reinforcement ratios. The average ρ of the means of the five buildings is 0.0043. The largest mean ratio is 0.0057 for CM building and the lowest mean ratio is 0.0022 for AH building

Table 3.3. Vertical boundary reinforcement ratio of walls of the damaged buildings

Building	**Mean**	**Max**	**Min**	**St. Deviation**
CM	0.0057	0.0123	0.0009	0.0032
AH	0.0022	0.0051	0.0004	0.0011
PR	0.0045	0.0089	0.0005	0.0030
AA	0.0040	0.0096	0.0016	0.0019
EM	0.0051	0.0086	0.0008	0.0030
	0.0043	**0.0123**	**0.0004**	**0.0025**

The vertical distributed reinforcement ratios (ρ_l) of the walls of damaged buildings are summarized in Table 3.4, where the average ratio of the five buildings is 0.0108. AH building has the highest average ratio (0.0249) and the maximum ratio in a single wall is 0.0327, which is about 13 times the minimum reinforcement ratio of 0.0025 required by the ACI 318-11 (2011). The high average ρ_l in building AH seems to compensate the low average ratio of vertical boundary reinforcement (ρ=0.022 in Table 3.3). EM building also has a high ρ_l=0.0134 compared to the other three buildings (CM, PR and AA) whose average is 0.0053.

Table 3.4. Vertical distributed reinforcement ratio of walls of the damaged buildings

Building	Mean	Max	Min	St. Deviation
CM	0.0061	0.0224	0.0025	0.0061
AH	0.0249	0.0327	0.0169	0.0065
PR	0.0050	0.0168	0.0027	0.0048
AA	0.0048	0.0268	0.0020	0.0070
EM	0.0134	0.0236	0.0075	0.0063
	0.0108	**0.0327**	**0.0020**	**0.0061**

The horizontal reinforcement ratios (ρ_t) of the walls of the damaged buildings are summarized in Table 3.5, where the average ratio of the five buildings is 0.0045 which is about 1.8 times the minimum reinforcement ratio of 0.0025 required by the ACI 318-11 (2011). Table 3.5 shows that the standard deviation is relatively small, the maximum ratio is 0.0151 in PR Building and the minimum ratio is 0.0025 in CM and AA.

Table 3.5. Horizontal reinforcement ratio of walls of the damaged buildings

Building	Mean	Max	Min	St. Deviation
CM	0.0032	0.0039	0.0025	0.0005
AH	0.0068	0.0075	0.0052	0.0011
PR	0.0050	0.0151	0.0033	0.0041
AA	0.0032	0.0057	0.0025	0.0009
EM	0.0043	0.0062	0.0025	0.0015
	0.0045	**0.0151**	**0.0025**	**0.0016**

From the described survey it can be summarized that the thickness of the walls from damaged buildings varied from 15 cm to 25 cm and the average M/Vl_w ratio was 2.02, which implies that flexural behavior was relevant. The walls were subjected to relatively high ALRs which made them susceptible to brittle compression controlled behavior. The walls were provided with large vertical reinforcement ratios to provide strength but inadequate confinement was provided. The average wall properties of each of the five damaged buildings studied are shown in Table 3.6

Table 3.6. Average wall properties of damaged buildings

Building	$\frac{M}{Vl_w}$	**D+L ALR**	**D+L+E ALR**	ρ	ρ_l	ρ_t
CM	2.96	0.16	0.24	0.0057	0.0061	0.0032
AH	1.36	0.17	0.28	0.0022	0.0249	0.0068
PR	2.35	0.13	0.27	0.0045	0.0050	0.0050
AA	2.23	0.11	0.19	0.0040	0.0048	0.0032
EM	1.19	0.29	0.34	0.0051	0.0134	0.0045
Average	**2.02**	**0.17**	**0.26**	**0.0043**	**0.0108**	**0.0045**

3.3 Analytical Study of Selected Wall

An analytical study of one of the RC walls considered in the previous survey, which failed during the earthquake, is described in this section. This analysis is aimed to explain the observed damage. The wall is located in CM building and the failure is shown in Figure 3.6, where a horizontal region of concrete crushing and longitudinal bars buckling is observed. This flexural-compressive failure mode seems to be attributed to high axial loads, poor confinement and inadequate transverse reinforcement detailing.

The selected wall is located in the second story in axis 'E' (Figure 3.7) of CM building which was designed with H30 concrete ($f_c' = 25\,MPa$) and A630-420H steel (f_y=

$420\ MPa\ and\ f_u = 630MPa$). The period of the CM building in the Y-axis (direction of the E axis and the selected wall) and in the X-axis are 0.8 sec and 0.56 sec, respectively. The length of the selected wall is 220 cm, the thickness 20 cm, the cross section 2.67 m^2, and the story height 2.6 m. The building has a significant irregularity; the floor area of the second story is considerably larger than that of the first story. Therefore, high loads are concentrated in walls of the second story. In order to resist these high loads, this wall was strengthened with additional 28 ϕ 12 mm vertical bars in the second story. These bars were added in between the vertical reinforcement of 30 ϕ 16 mm bars that this wall has along the height of the building (Figure 3.8). The transverse reinforcement consists in ϕ 10 mm bars spaced at 20 cm. These reinforcement results in reinforcement ratios of ρ_l=0.021 and ρ_t=0.0040. The s/d_b ratio is 16.7, where s is the spacing between transverse bars and d_b is the diameter of the smallest longitudinal bar. This high s/d_b ratio suggests that reinforcement bar buckling should have happened immediately in the next compressive cycle after yielding in tension (Monti & Nuti, 1993; Rodriguez et al., 1999).

Figure 3.6. Observed failure in selected wall

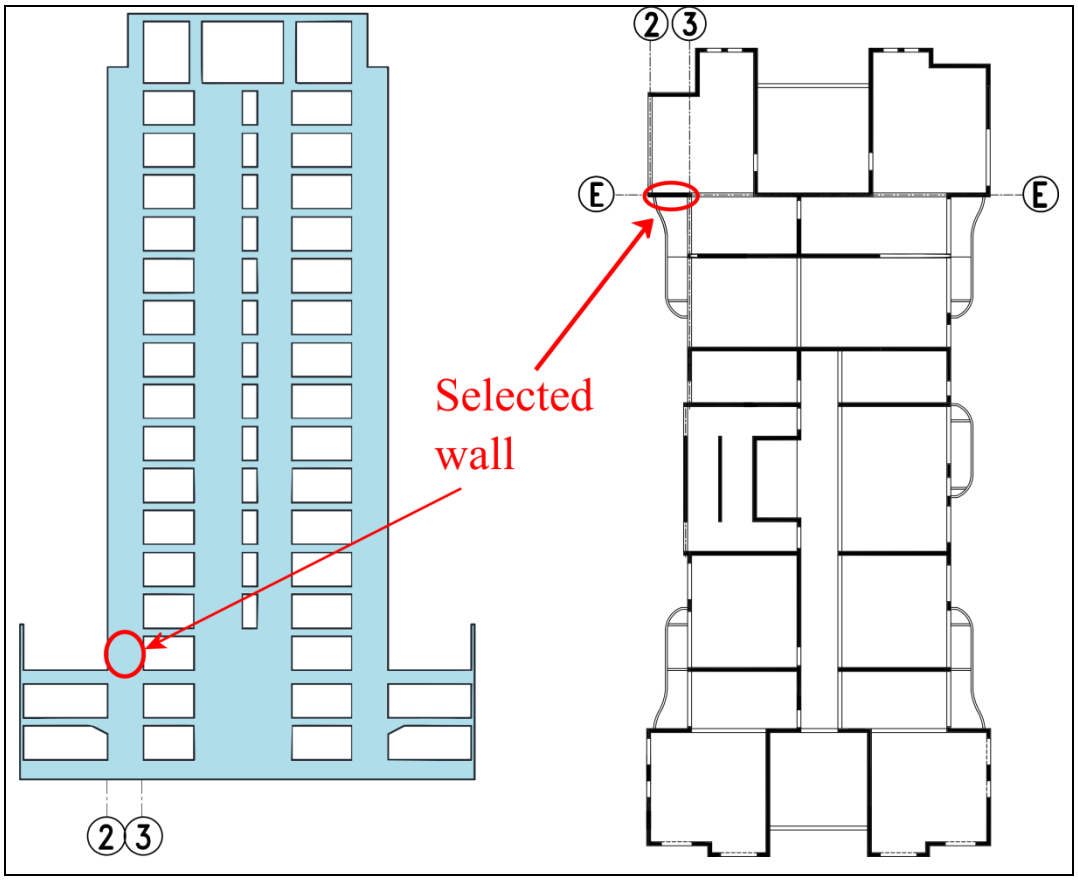

Figure 3.7. Elevation view of axis E from CM building and Plan view of second story from CM building

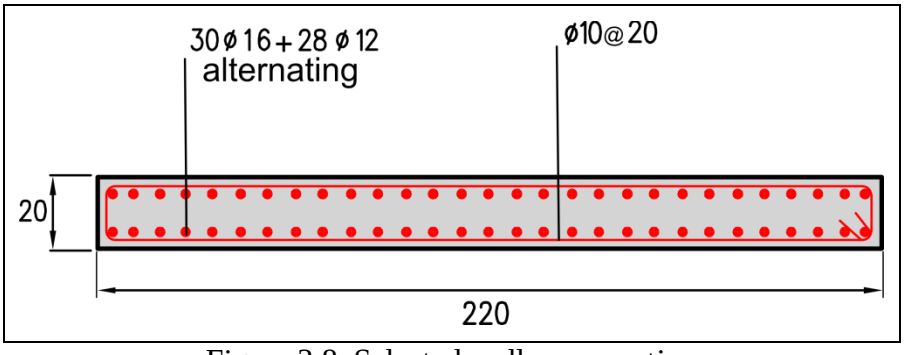

Figure 3.8. Selected wall cross section

A fiber-model for RC sections was developed in MATLAB (Mathworks, 2010) in order to obtain the moment-curvature relationships of RC walls. The stress-strain constitutive models for concrete and steel were the ones proposed by Karthik & Mander (2011)

where the model for concrete in compression depends on the confinement reinforcement of the section. Because of the lack of confinement in the selected wall, low effective confining stresses are obtained in the section following Mander's procedure (Mander et al., 1988). The highest confinement stress in the selected wall is less than 0.1% of the concrete strength, thus, the resulting confinement ratio is $K = 1.0$. Therefore, only unconfined concrete was considered in the model (Figure 3.9). The peak and ultimate stresses of the concrete are 25 MPa and 12 MPa at strain levels of 0.0019 and 0.0036 respectively, and a failure strain of 0.0095 was considered for concrete. For the reinforcing steel (Figure 3.9), nominal properties were considered with f_y= 420 MPa, f_u= 630 MPa and a modulus of elasticity of 200,000 MPa. Additionally, a strain hardening modulus of 5,000 MPa, a hardening strain of 0.01 and an ultimate strain of 0.16 were considered. These last three parameters were obtained from average properties of the reinforcing bars tested for the experimental campaign conducted as part of this research project (Appendix A.2).

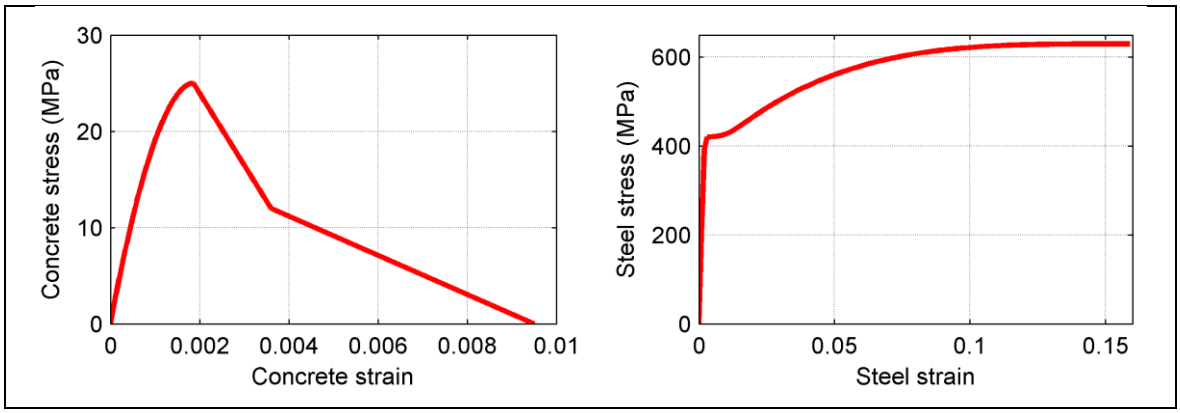

Figure 3.9. Material stress-strain relations (Karthik & Mander, 2011)

The axial loads of the wall were obtained from the finite element model of the building using ETABS (Computers & Structures, 2011). The wall is subjected to axial loads of 1364 kN, 265 kN and 1775 kN for dead, live and earthquake loads, respectively. The earthquake load is obtained from a modal spectral analysis following NCh433 code (INN, 2009). The shear load and the bending moment at the base of the wall in the second story for the earthquake loads are 153 kN and 266.6 kN-m, respectively.

Therefore, the M/VL_w ratio is 0.67. This small ratio suggests that the wall behavior should be controlled by shear action. However, the failure (Figure 3.6) does not show diagonal shear cracks, but shows an horizontal failure which is induced by concrete crushing and vertical bar buckling. The total axial load of the wall under service condition during an earthquake is estimated as $P_D + 0.25\,P_L + P_E = 3205$ kN, which is equivalent to an ALR of 0.29.

Considering ALRs of 0.1, 0.2 and 0.3 (axial loads of 1,100 kN, 2,200 kN and 3,301 kN respectively) and the described material properties, the moment curvature relationship was computed for the wall section (Figure 3.10). The moment curvature relation that corresponds to 0.3 ALR can be supposed as the behavior of the selected wall.. The yield curvature is estimated as 1.8E-05 1/cm and the ultimate curvature as 7.5E-05 1/cm. Therefore, the estimated curvature ductility of the wall is only 4.14 and a negative slope in the moment curvature relationship is predicted beyond the peak moment strength of 4310 kN-m. This curvature ductility is relatively small and is not consistent with the load reduction factor (R*) of 6.42 that is used in the transverse direction according to NCh433 (2009).

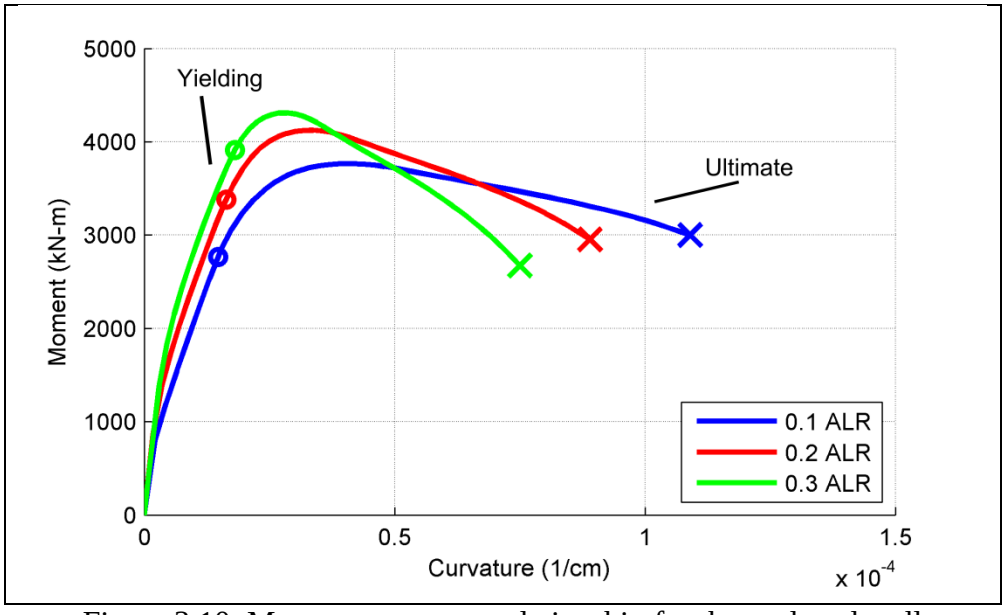

Figure 3.10. Moment-curvature relationship for the analyzed wall

The strength of the selected wall was verified according to NCh433 (INN, 2009), where the earthquake loads are obtained from a modal spectral analysis and the ultimate loads are obtained using the load combinations of NCh3171 (INN, 2010). The interaction diagram of moment and axial load of the selected wall (Figure 3.11) shows that the ultimate loads are smaller than the factored capacity, thus, the wall was designed adequately. Additionally, the design earhquake at the fundamental period of the building (0.8 sec) was comparable to the ground motions recorded at the vecinity of the building. The factored pseudo acceleration for soil type III, which was the soil classification of the building, is $1.4 \cdot 1.05g = 1.47g$, which is 12% larger than the maximum pseudo acceleration from the two ground motion recorded at the vecinity of the building (1.3g for San Pedro Ground motion NS compoment; Figure 3.12).

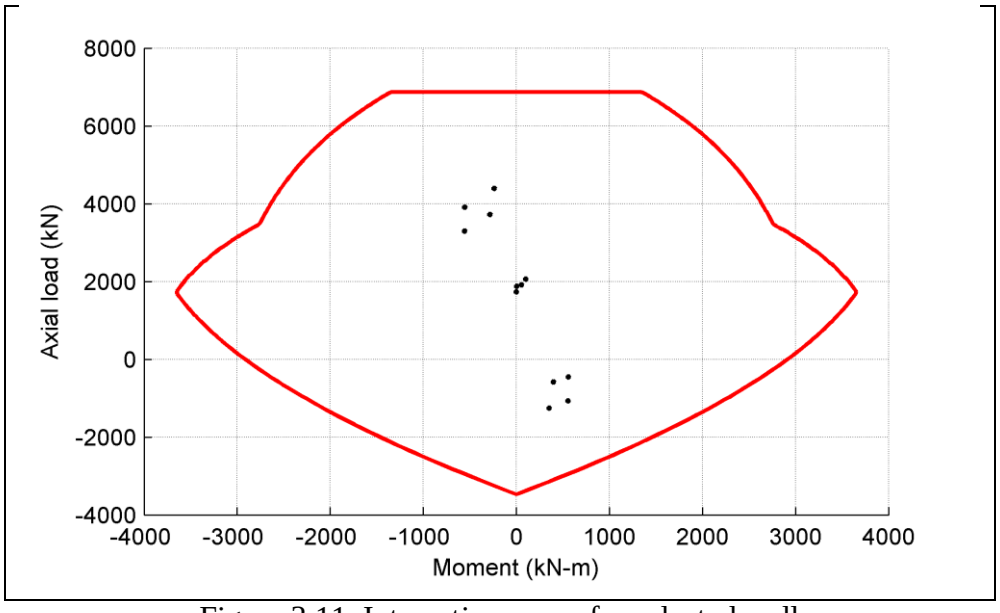

Figure 3.11. Interaction curve for selected wall

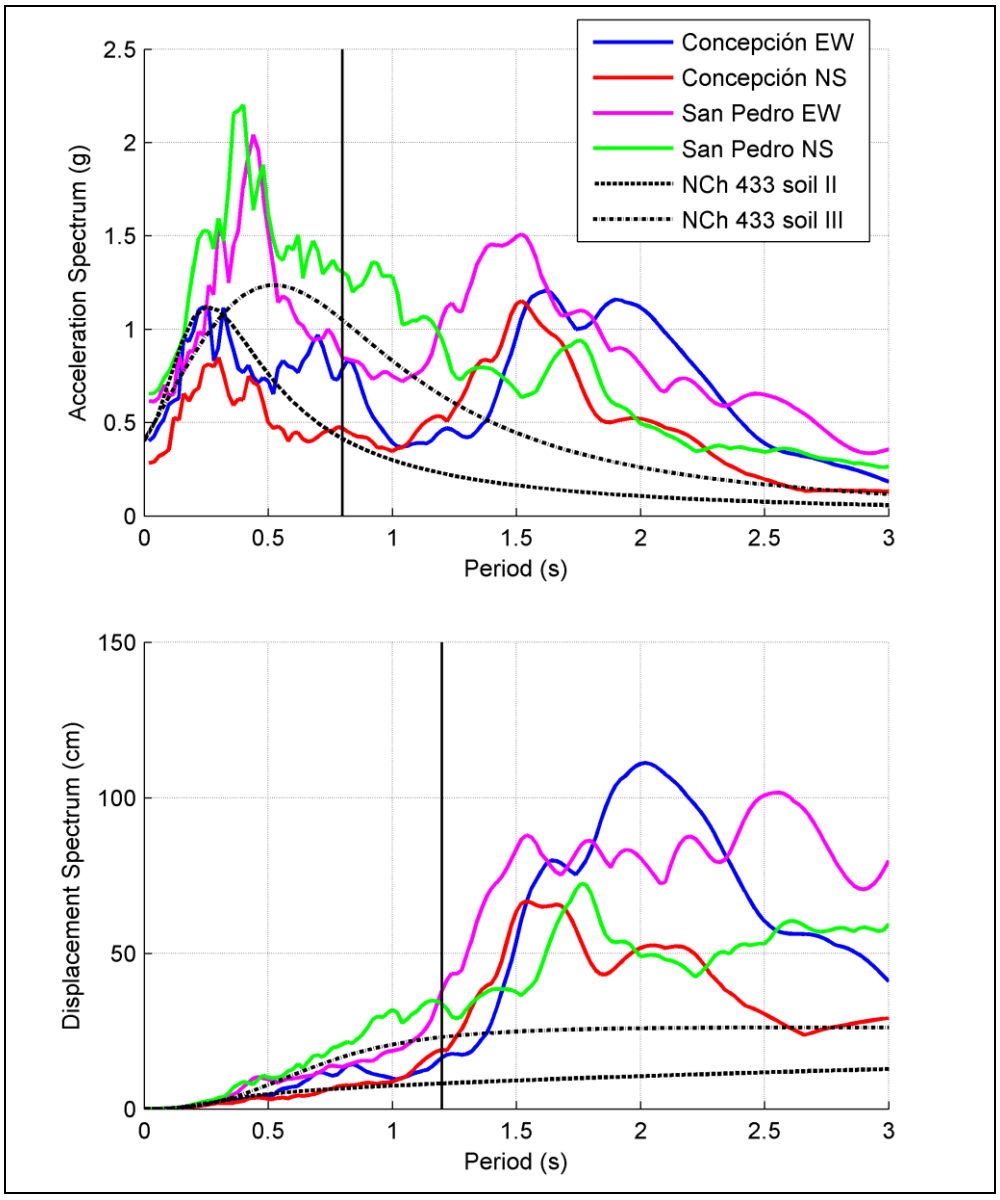

Figure 3.12. Pseudo-Acceleration and displacement spectrum for 2010 ground motions and NCh 433 (INN, 2009) spectrum

A plastic hinge approach was used to estimate the roof displacement capacity of the building considering a wall height of 40.70 m (h_w) measured from the bottom of the second story to the roof (Figure 3.13(a)). If a plastic hinge length of $Lp = L_w/2 = 110$ cm is considered, the yield and ultimate roof displacement are 99.9 cm (2.46% drift) and 125.1 cm (3.07% drift) respectively, and the provided displacement ductility is 1.25.

The estimated roof displacement demand for the E-W direction (same as the axis of the selected wall) of CM building during 2010 Earthquake is 49.1 cm. This displacement is estimated as $\delta_u = 1.3\, S_d(T_{cr})$ following DS 61 (2011) recommendations. In this calculation S_d is obtained from the maximum displacement spectra of the two ground motions recorded near the building (Figure 3.12) considering T_{cr} = 1.2 s (1.5 times T_y = 0.8 s). From this analysis it can be conlcuded that the roof displacement capacity of the wall using the plastic hinge approach is 2.5 times the displacement demand. This is not consistent with the failure of the wall and the plastic hinge approach does not correlate with the oberved damage.

The ACI318 (2011) approach to estimate the roof displacement of a cantilever wall is shown in Figure 3.13(b) where the elastic cuvature is neglected. If the displacement demand (δ_u = 49.1 cm) is considered in this equation, the curvature demand for the wall is φ_u = 1.09E-04 1/cm, which is impossible to attain for this wall whose ultimate curvature is estimated as 7.5E-05 1/cm. If the ALR of this wall is reduced from 0.29 to 0.1, the ultimate curvature capacity increases to 1.09E-04, and the displacement demand is possible to attain in this case. However, Wallace et al. (2012) suggests that for poorly detailed walls, which is this case, the plastic hinge length should be smaller than $L_w/2$. Hence, considering a platic hinge length of $Lp = 2.5\ tw = 50$ cm, which resulted in an accurate prediction for the ultimate displacement for Takahasi et al. (2013), the curvature demand increases to 2.4E-04 1/cm, which is impossible to attain for the selected wall even in the case with ALR of 0.1. This analysis shows that considering that the wall failed, the ACI approach for estimating the roof displacement capacity of a wall of a Chilean building seems to be more realistic than the platic hinge approach. Although the wall satisfy the design strength requirements, it is not able to sustain the displacement demand from the 2010 Earthquake. It is important to highlight the high potentitial for bar buckling of this wall ($s/d_b = 16.7$) which was not considered in the fiber model. The cyclic loading during the earthquake should have triggered an early bar buckling on the onset of yielding, which results an even more brittle and dangerous behavior than that predicted by the fiber model.

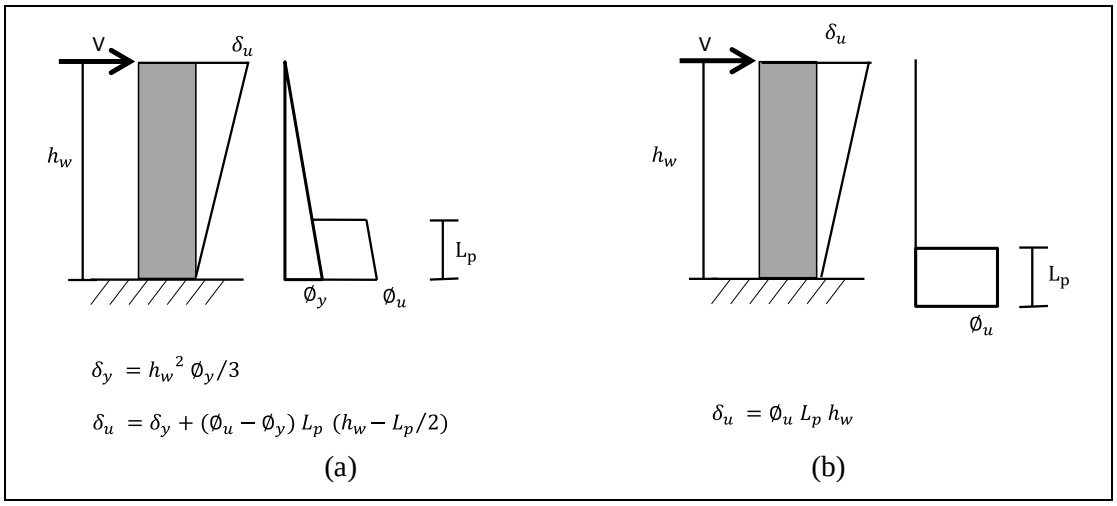

(5)

Figure 3.13. (a) Plastic hinge and (b) ACI318 approach for estimation of roof displacement of a cantilever wall

The analysis performed for the selected wall suggest that the strength provided to the wall was adequate according to the seismic code and that the actual ground shaking was comparable to that of the design code. However, the provided ductility was not consistent with the load reduction factor used in the design of the building. The high ALR, the inadequate concrete confinement, and the lack of restrain for longitudinal bar buckling compromised the displacement capacity of walls and a brittle compressive damage was generated.

4. EXPERIMENTAL PROGRAM

Three identical RC wall specimens (W1, W2 and W3) were designed with representative characteristics obtained from the survey of RC walls from damaged buildings performed in Chapter 3. The design and construction of the wall specimens and the test setup including instrumentation and load application protocol are described in this Chapter. Double-cycle displacements with increasing amplitude and constant ALR of 0.15, 0.25 and 0.35 were applied to specimen W1, W2 and W3 respectively in order to reproduce the observed failure in walls during the 2010 Chile Earthquake and evaluate the influence of axial load in the seismic behavior of the walls.

4.1 Specimen Design

Based on the survey of walls from damaged buildings conducted in Chapter 3 a prototype RC wall was defined for conducting the experimental program. A ½-scale was selected for the wall prototype due to the maximum loads that can be applied with the available equipment at Pontificia Universidad Catolica de Chile. The wall cross section is 70 cm wide, 10 cm thick and the wall height is 160 cm. Thus, the h/l_w ratio of the wall prototype is 2.3. The wall is designed with base and top RC beams to connect it to the loading frame. The base beam is 140 cm wide, 40 cm thick and 42.5 cm high. The top beam is 70 cm wide, 30 cm thick and 30 cm high. The geometry of the wall specimen is shown in Figure 4.1. The lateral load was applied at mid height of the top beam (at 175 cm from the base), therefore, the resulting M/Vl_w ratio of the wall specimen is 2.5. This ratio is slightly higher than the average ratio of the walls from the survey but it is perfectly in the actual range in practice and also was selected in order to ensure a flexural-compressive mode of failure as observed in most damaged walls during the 2010 Chile Earthquake. Squat unconfined Chilean walls have already been studied by Hidalgo et al. (2002) and thus a shear failure mode is intended to be avoided in this project.

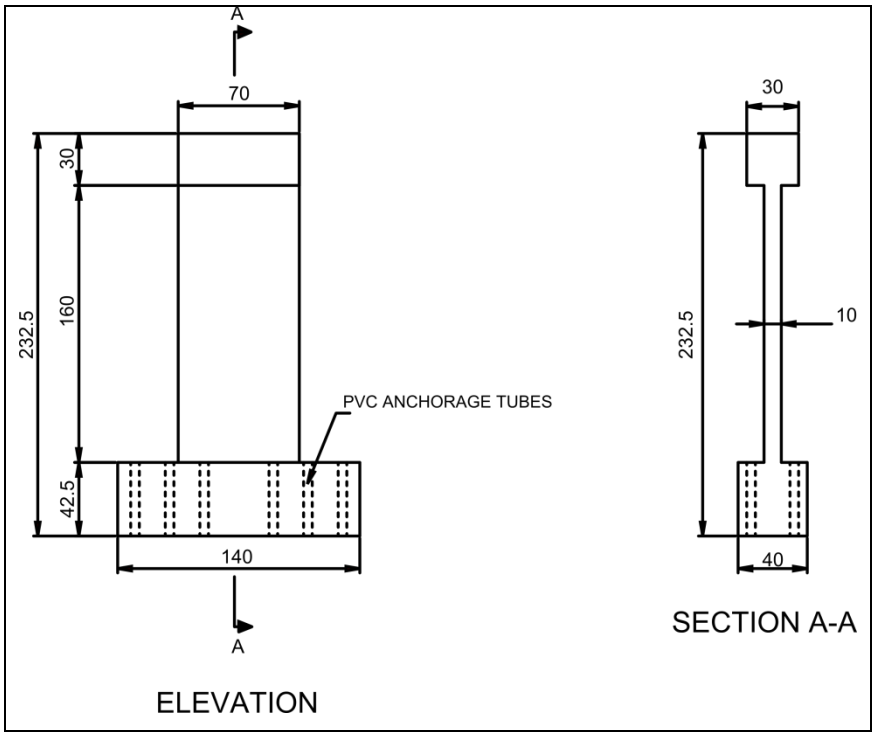

Figure 4.1. Wall specimens geometry (in cm)

The vertical boundary reinforcement is 2+2 ϕ10 mm (ρ=0.0045) and the distributed reinforcement is ϕ8 mm bars spaced at 140 mm (ρ_l=0.0072). For the horizontal distributed reinforcement ϕ5 mm bars spaced at 90 mm (ρ_t=0.0044) are used. The selected reinforcement results in an s/d_b ratio of 9 which is within the typical range of 8 to 11 in Chilean walls (Wallace et al., 2012). Additionally, 8 ϕ5 ties in the central vertical bar are distributed uniformly throughout the height of the wall in order to follow Chilean construction practice. The reinforcement ratios for vertical boundary and horizontal reinforcement ratio are similar to the average ratios obtained from the survey of damaged walls (Table 3.3 and Table 3.5). The ratio of the vertical distributed reinforcement is smaller than the average of the survey, because the mean ratios of two buildings are considered excessively high compared to the other three buildings (Table 3.4). Therefore, a ratio of 0.0072 seems to be reasonable for the vertical distributed reinforcement. The reinforcement detailing of the wall specimens is shown in Figure 4.2. The horizontal reinforcement detailing follows typical construction practice in Chile which consists on hoops with 90-degree hooks outside the vertical bars which are not

anchored into the concrete core and become ineffective after spalling of concrete cover (Wallace et al., 2012). The reinforcement detailing of the base and top beams, not detailed in Figure 4.2, consist on ϕ12 mm longitudinal bars with intermediate ϕ10 longitudinal bars and ϕ8 mm stirrups spaced at 10 cm. A summary of relevant characteristics of the surveyed walls and the specimens are shown in Table 4.1.

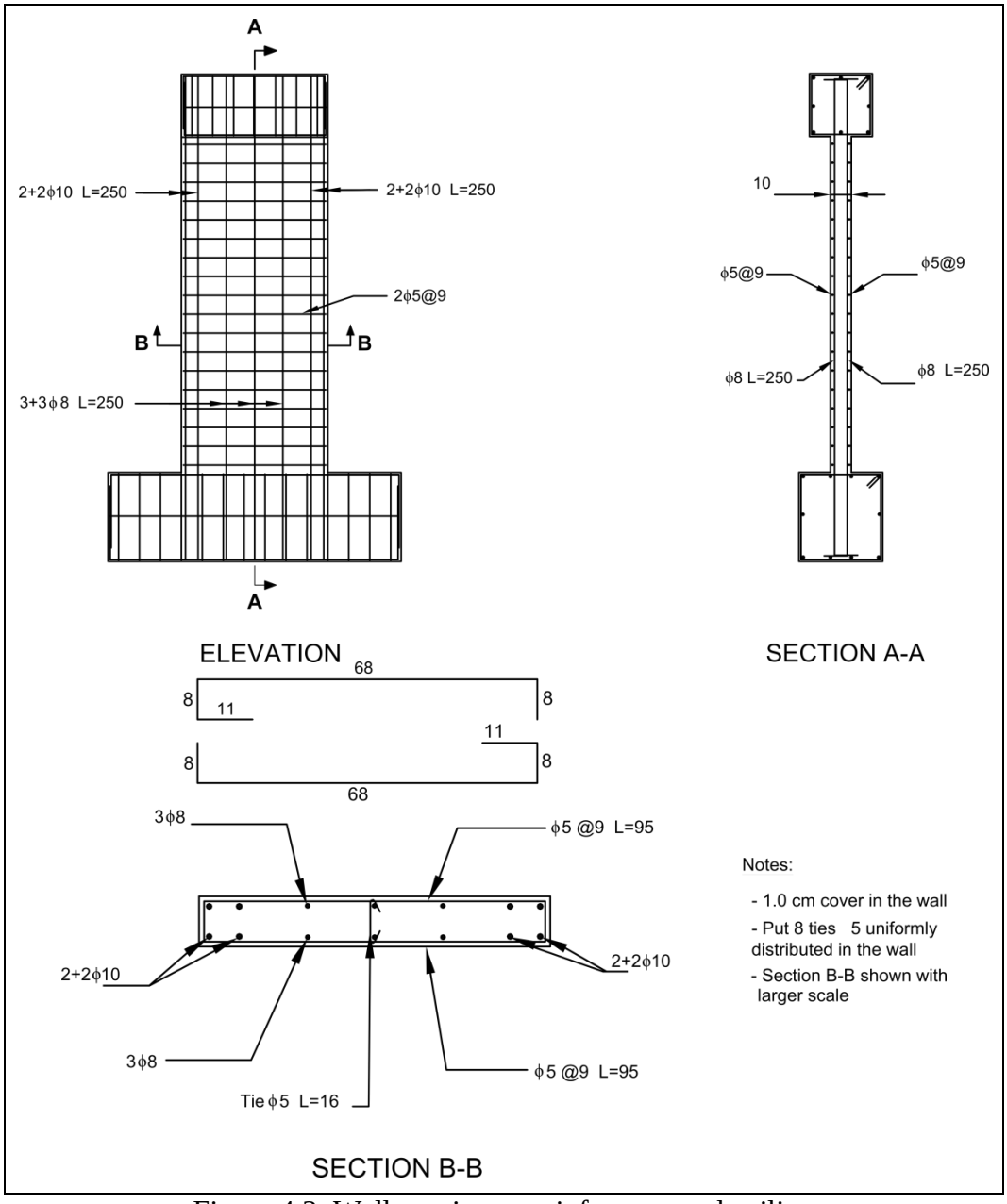

Figure 4.2. Wall specimens reinforcement detailing

Table 4.1. Characteristics of the surveyed walls and wall specimens

Property	Average	Max	Min	St. Deviation	Specimens
M/Vl_w ratio	2.02	11.67	0.19	2.01	**2.5**
ρ	0.0043	0.0123	0.0004	0.0025	**0.0045**
ρ_l	0.0108	0.0327	0.0020	0.0061	**0.0072**
ρ_t	0.0045	0.0151	0.0025	0.0016	**0.0044**

4.2 Wall Specimens Construction

A total of 11 wall specimens were built in the laboratory of the Structural and Geotechnical Engineering Department at Pontificia Universidad Católica de Chile. Three of these walls are part of this thesis which is aimed to study the effect of axial load and their design was described in Section 4.1. The other eight walls are not part of this thesis and were built to study the effect of other parameters such as wall thickness, M/Vl_w ratio and reinforcement detailing. Pictures of the construction process are shown in Figure 4.3. The wall specimens were built with wooden formwork and the steel bars were bent at the construction site. The concrete of the bottom bases was cast at the construction site using a mixer. Eight days later, the concrete of the walls and top bases was cast using pre-mixed concrete. The specimens were cured with plastic for 7 days at both stages and the finished walls are shown in Figure 4.4.

(a) Wooden formwork

(b) Folding of base reinforcement

(c) Reinforcement of walls

(d) Reinforcement of walls and beams

(e) Wooden formwork assembled

(f) Pre-mixed concrete truck

Figure 4.3. Wall specimen construction process

Figure 4.4. Wall specimens W1, W2 and W3

4.3 Material Properties

The concrete of the wall specimens was specified with a characteristic strength of 20 MPa and with a maximum aggregate size of 11 mm. For the reinforcement, A630-420H steel (f_y= 420 MPa) was specified for ϕ8, ϕ10 and ϕ12 mm bars, and AT560-500H steel (f_y=500 MPa) for ϕ5 mm bars. The properties of concrete and steel were measured in laboratory tests and were considered for the stress strain relations in the pre-test analysis of Chapter 5.

For concrete, cylindrical samples with 10 cm diameter and 30 cm height were tested in the laboratory in order to obtain its compressive strength. The details of the test are shown in Appendix A.1. The average concrete strength after 7 and 28 days was f_{c7} = 14.4 MPa and f_{c28} = 24.1 MPa respectively. Five larger cylindrical samples with 15 cm diameter and 30 cm height were also tested a day before the first test (260 days after specimen construction) where the average concrete strength was f_c' = 27.4 MPa. This strength is considered as the compressive concrete strength for the axial loads applied in the tests and for the analytical predictions in Chapter 5.

For reinforcing steel (Appendix A.2), three ϕ 8 mm and three ϕ 10 mm bars of A630-420H were tested in order to obtain the properties of the vertical bars. Also, three ϕ 5 mm bars of AT560-500H, which were used for the horizontal reinforcement, were tested. The average yield strength, ultimate strength, yield strain, hardening strain, ultimate strain, and strain hardening modulus of each bar type are summarized in Table 4.2. The yield strain was not measured in the test and was considered as $f_y/205{,}000\,MPa$ in order to use the same modulus of elasticity for all the steel specimens. The ϕ 5 mm AT560-500H bars are not ductile as the A630-420H steel bars, and strains during test were difficult to measure, hence, only yield strength and ultimate strength and ultimate strain are shown for ϕ 5 mm bars in Table 4.2.

Table 4.2. Average parameters for AT560-500H (ϕ 5) and A630-420H (ϕ 8 and ϕ 10)

Parameter	**ϕ 5 mm**	**ϕ 8 mm**	**ϕ 10 mm**
Yield strength (MPa)	608.9	445.6	469.2
Ultimate strength (MPa)	667.7	598.9	675.7
Yield Strain	-	0.0022	0.0023
Hardening strain	-	0.0139	0.0138
Ultimate strain	0.057	0.151	0.166
Strain hardening modulus (MPa)	-	4133.6	5430.9

4.4 Test Setup

The aim of the proposed tests is to apply different levels of constant axial load and equal cyclic incremental lateral loads to each wall specimen. To achieve this, the wall specimens were placed in a steel loading frame. The test setup is shown in Figure 4.5 and Figure 4.6 where the wall is fixed at the base and pinned at the top. The base beam was fixed to the strong floor in order to simulate a rigid foundation (Figure 4.7). The

horizontal 500kN actuator was pinned at its two sides and was attached to the top RC beam with 4 steel bars that were bolted against 400 x 300 x 30 mm steel plates at each side of the specimen. This connection (Figure 4.8) could transfer the lateral load reversals. At the other end, the horizontal actuator was supported by a steel IN beam which was bolted to the steel frame. As the horizontal load was applied at the center of the top beam, the effective height of the wall specimen is 175 cm. A 50 kN concrete counterweight was connected to the clevis of the horizontal actuator at the specimen side using two pulleys. This counterweight was used to hang the actuator and eliminate the vertical reaction induced by the actuator weight in the specimen. The vertical 700 kN actuator was bolted to the steel frame and connected to the specimen using rollers to allow horizontal displacement of the top beam (Figure 4.9). Therefore, the P-delta effect was included in the test setup. The out-of-plane displacement of the wall specimens was restrained with rolling supports that were connected to a steel I beam at each side of the top beam (Figure 4.5).

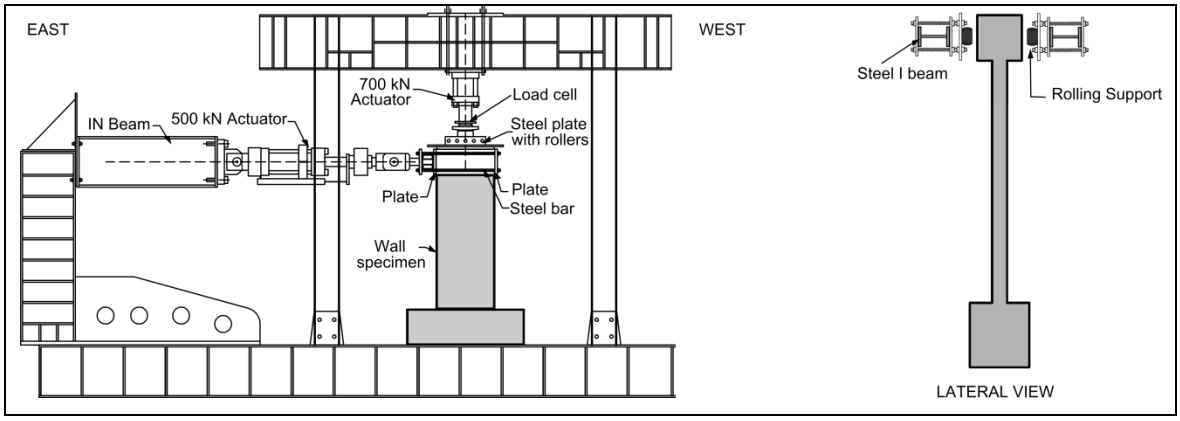

Figure 4.5. Test setup. Lateral view shown in higher scale.

Figure 4.6. Test Setup (picture)

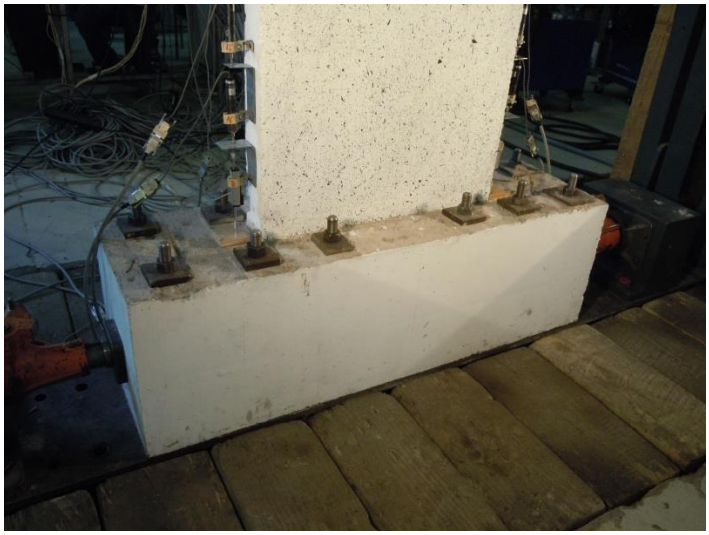

Figure 4.7. Fixed base beam for wall specimens

Figure 4.8. Horizontal actuator attached to the top beam

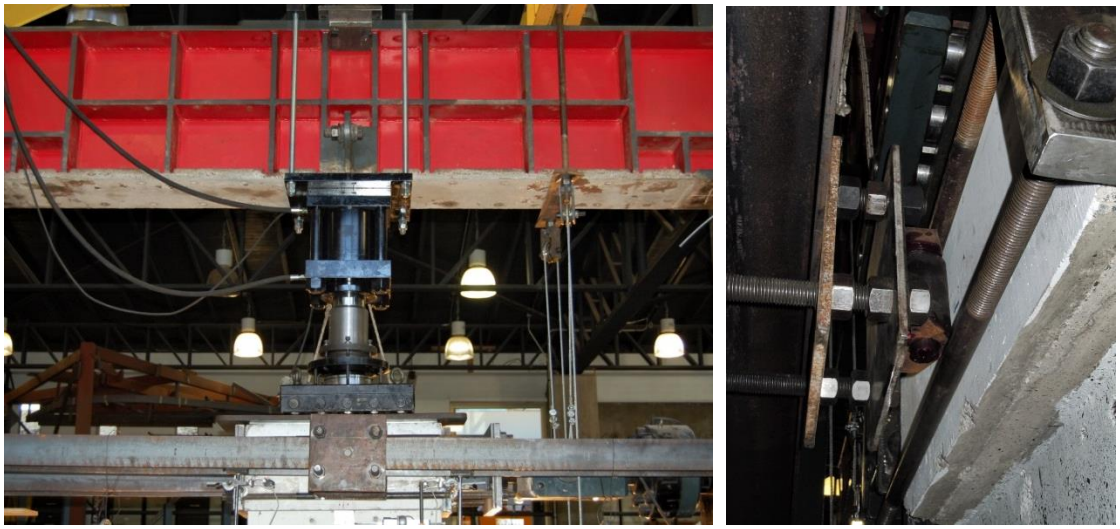

Figure 4.9. Vertical actuator and rolling supports

4.5 Instrumentation

The specimens were instrumented with 2 load cells, 14 displacement transducers, and 16 strain gauges attached to the reinforcement bars, and also using a photography camera to conduct image correlation processing in future studies. Loads cells were connected to both horizontal and vertical actuators in order to measure the applied loads. The displacement transducers were installed in the wall specimens to measure displacements and to obtain curvatures. The channel configuration and list of load cells and displacement transducers are shown in Figure 4.10 and Table 4.3, respectively. The strain gauges were used in each specimen to measure strains in the reinforcing steel bars and were installed during the construction of the wall specimens. The strain gauge configuration is shown in Figure 4.11 where V1, V2, V3, V4, V5, V6 and V7 were installed in the vertical bars through the wall length; V1M, V1T, V7M and V7T were installed at the boundary vertical bars to measure strains at higher levels of V1 and V7 bars respectively; and H1E, H1W, H2E, H2W and HT were installed in the horizontal steel bars. For the image correlation method, the wall was painted with small black spots (Figure 4.12) and a high resolution digital camera was installed at the north of the specimen. The camera took pictures during the tests every 5 seconds and adequate light was provided to the specimen. The MATLAB (MathWorks, 2010) image correlation toolbox was used to process the pictures and measure displacements along time.

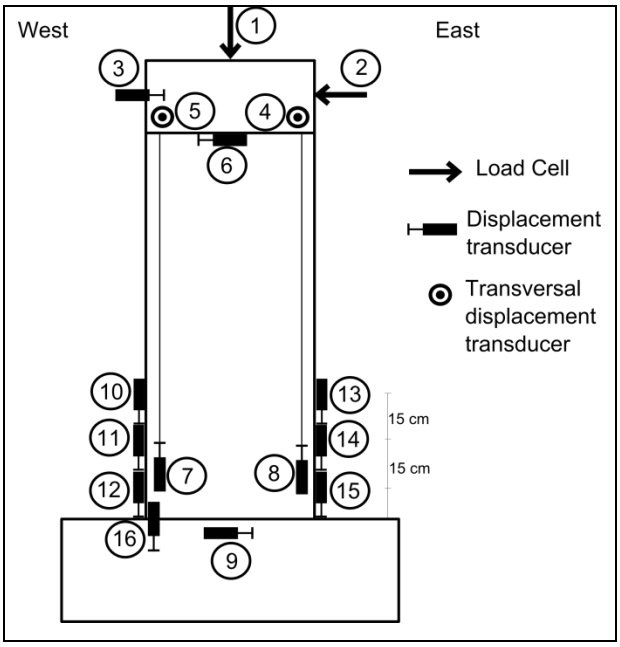

Figure 4.10. Load cell and displacement transducer channel configuration

Table 4.3. Load cell and displacement transducer channel list

Channel	**Measure**	**Channel**	**Measure**
1	Vertical load	9	Horizontal base displ.
2	Horizontal load	10	Superior curvature (West)
3	Horizontal displacement at h=1.75 m	11	Central curvature (West)
4	Out of plane displacement (East)	12	Inferior curvature (West)
5	Out of plane displacement (West)	13	Superior curvature (East)
6	Horizontal displacement at h=1.60 m	14	Central curvature (East)
7	Top beam vertical displ. (West)	15	Inferior curvature (East)
8	Top beam vertical displ. (East)	16	Vertical base displ.

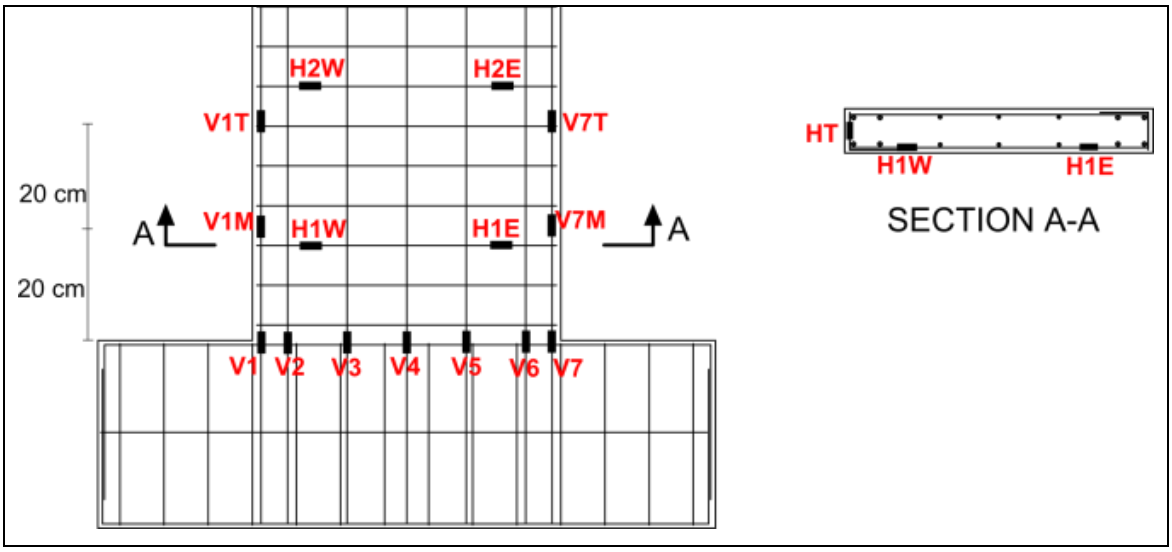

Figure 4.11. Strain gauge configuration

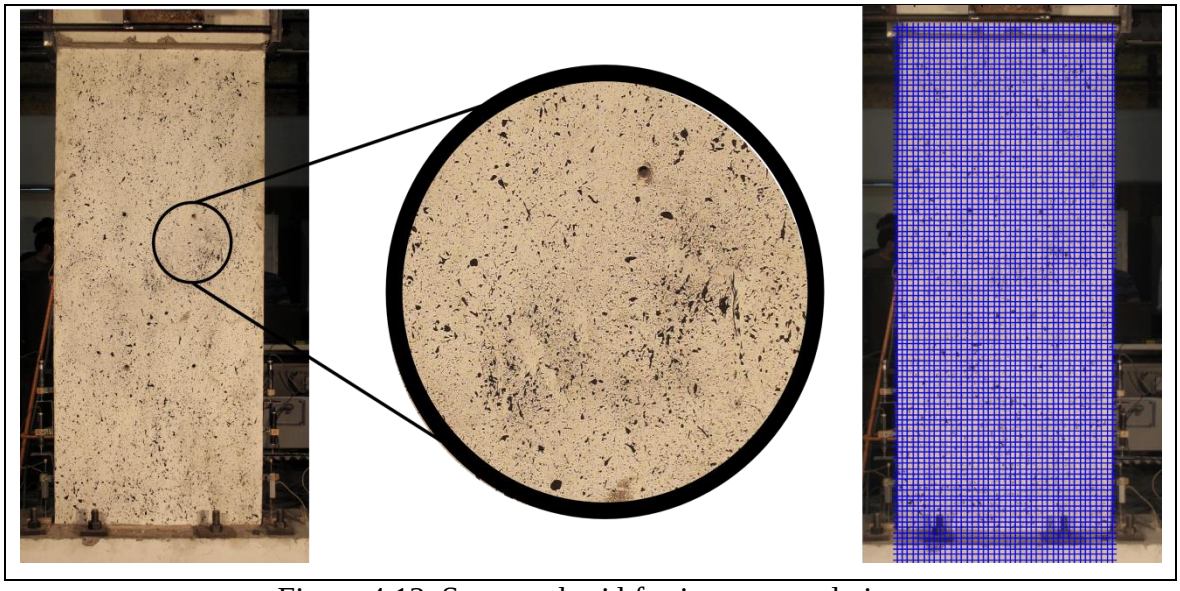

Figure 4.12. Spots and grid for image correlation

4.6 Load Application and Control

Constant axial load and increasing lateral displacements were applied to the wall specimens in the three tests. This section shows how this load and displacement programs were designed. According to the survey of damaged walls (Chapter 3; Figure 3.5) and the maximum loads that can be supported by the available equipment, the three walls were tested with different ALRs: 0.15, 0.25 and 0.35. Table 4.4 shows the ALR and the axial load in the three wall specimens.

Table 4.4. Applied axial loads for wall specimens

Specimen	**ALR (N/f'_cA_g)**	**Axial Load (kN)**
W1	0.15	287.4
W2	0.25	479.0
W3	0.35	671.6

The three wall specimens were subjected to a constant vertical load that was maintained through the test by controlling the hydraulic pressure. Following the application of the axial load, the wall specimens were subjected to double-cycle horizontal displacements with increasing amplitude. The horizontal displacement was applied at a constant velocity of 10 mm/min.

The displacement cycles were designed based on the horizontal yield displacement of the wall specimen. The yield curvature can be estimated as: (Wallace et al., 2012)

$$\varphi_y = 1.5\ to\ 2.0\frac{\varepsilon_{sy}}{l_w} \tag{6}$$

Where $\varepsilon_{sy} = 0.0023$ is the yield strain of the ϕ10 A630-420H vertical bars (Table 4.2), and $l_w = 70\ cm$ is the length of the wall. Using equation (6) a yield curvature between

4.9E-05 and 6.5E-05 1/cm is obtained. Then, the yield displacement can be obtained from:

$$\delta_y = \frac{{h_w}^2 \varphi_y}{3} \tag{7}$$

Where $h_w = 175\ cm$ is the height of the free cantilever wall. A yield displacement between 5 and 6.5 mm is obtained using equation (7). A conservative approximation of $\delta_y = 5.5$ mm was considered for the yield displacement of the wall specimen. The ductility factors $\delta_{applied}/\delta_y$ that were intended to be applied to the three wall specimens walls in were 0.5, 1, 1.5, 2 ,3 ,4 ,5, 6 and 8. A previous test performed in the test setup with a similar wall specimen showed an average displacement loss of 20% (displacement measured for the wall specimen compared to the displacement of the actuator) which is attributed to the flexibility of the loading frame that supported the horizontal actuator. This displacement loss was higher in the first cycles and smaller in the last cycles. Thus, the horizontal actuator was commanded with displacement amplitudes 20% larger than the ones considering the estimated yield displacement (5.5 mm) of the wall. The commanded peak displacements were 3.3, 6.6, 9.9, 13.2, 19.8, 26.4, 33, 39.6 and 52.8 mm (Figure 4.13).

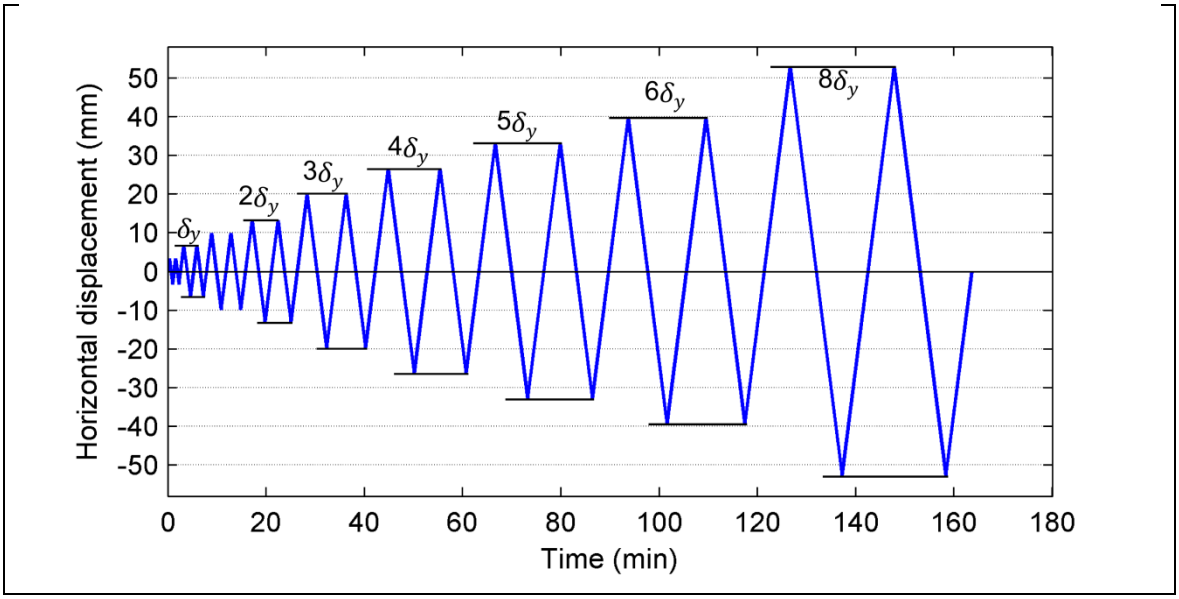

Figure 4.13. Horizontal displacement loading cycles

5. PRE-TEST ANALYSIS

Analytical calculations of the RC wall specimens were performed in order to estimate their strength and deformation capacity at different ALRs. The concrete and steel bars of the wall specimens were tested in section 4.3, in order to use real steel and concrete properties with realistic stress strain models to study the moment curvature relations.

5.1 Concrete Stress-Strain Relationship

The Karthik and Mander (2011) stress-strain model is considered for the behavior of confined and unconfined concrete. The compressive concrete strength considered in this model is f_c' = 27.4 MPa (section 4.3). As discussed in previous chapters, the wall specimens were designed with similar properties than walls from damaged Chilean buildings, hence the confinement is low. The confined concrete area of the wall section at the stirrups level is shaded in Figure 5.1 and at midway between stirrups the effective confined concrete area is only 3.3% of the concrete core (Mander et al., 1988). Based of the amount of horizontal reinforcement, the confinement ratio of this section is $K = f'_{cc}/f'_c = 1.01$, where f'_{cc} is the compressive concrete strength of the confined core. Table 5.1 shows the properties for unconfined and confined concrete and their constitutive models are shown in Figure 5.2, where the tensile strength of concrete is neglected.

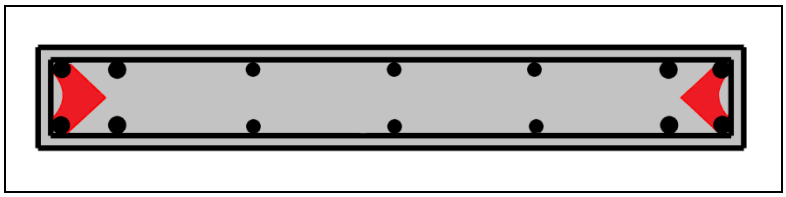

Figure 5.1. Confined concrete area at the stirrups level

Table 5.1. Parameters for unconfined and confined concrete

Parameter	Unconfined Concrete	Confined Concrete (K=1.07)
Peak Stress (MPa)	27.4	27.6
Peak Strain	0.0019	0.0020
Ultimate Stress (MPa)	12	12.3
Ultimate Strain	0.0036	0.010
Failure Strain	0.0093	0.014
Concrete Modulus (MPa)	26154	26154

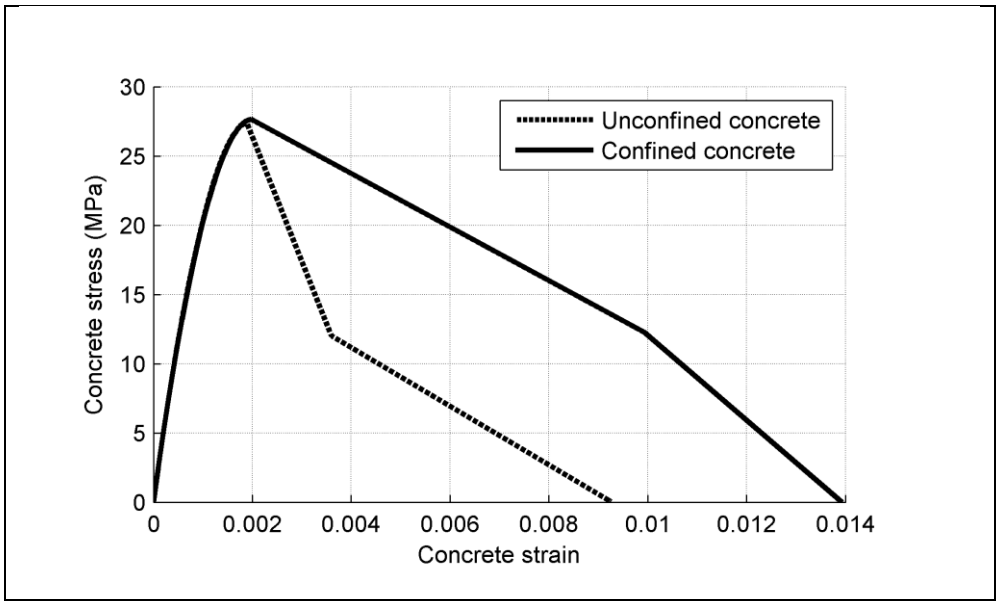

Figure 5.2. Concrete stress-strain relationships following Karthik and Mander (2011) model

5.2 Steel Stress-Strain Relationships

The realistic stress-strain model proposed by Karthink and Mander (2011) for reinforcing steel (Figure 5.3) was adopted using the average measured properties (Table 4.2). The modulus of elasticity was not measured in the test and E = 200,005 MPa is assumed. Thus, the yield strain for the ϕ10 bar, which is the most relevant as it is located near the wall edge, is 0.0023.

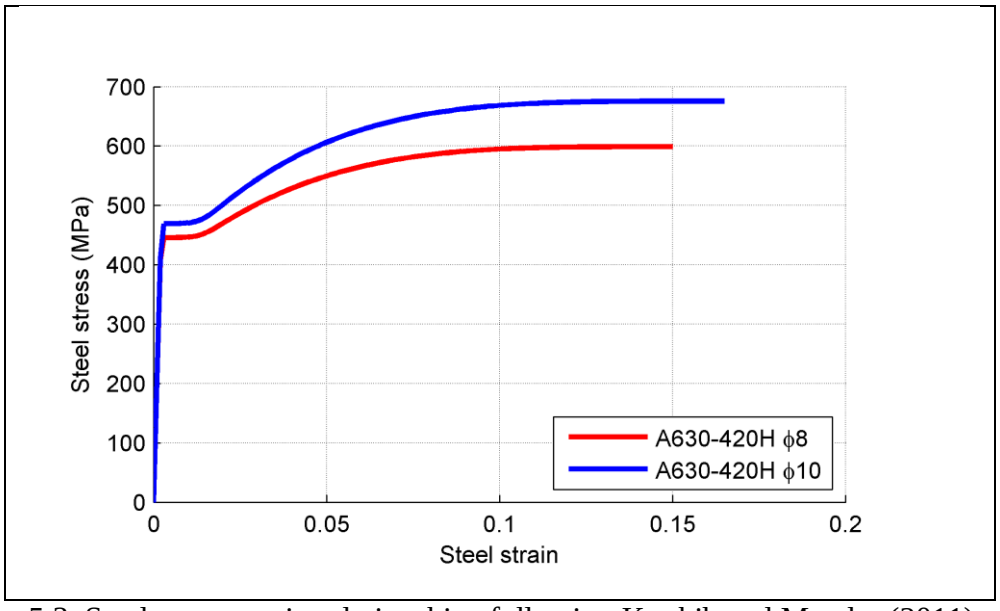

Figure 5.3. Steel stress-strain relationships following Karthik and Mander (2011) model

5.3 Wall ACI Strength

The nominal interaction diagram (Figure 5.4) and the shear stregth of the wall specimens were estimated according to ACI318 (2011) provisions. The concrete compressive strength and the steel yield strength obtained from the material tests results were considered for computing the interaction diagram and the shear strength. However, simple behaviors are considered for concrete and steel according to the ACI; stress block model for unconfined concrete was used for the concrete and an elastoplastic behavior was used for the steel.

The shear strenght of the wall specimens, V_n, was obtained using the ACI provisions from section 21.9.4 as:

$$V_n = A_w(\alpha_c \lambda \sqrt{f_c'} + \rho_t f_y) \leq 0.83 A_w \sqrt{f_c'} \quad (8)$$

Where, A_w = 700 cm is the wall cross section area, α_c = 0.17 for $hw/lw > 2$, λ = 1 for normal concrete and $\rho_t = 0.0044$ is the transverse reinforcement ratio. Therefore, using equation (8) the analytical shear strength of the three wall specimens is 248.3 kN.

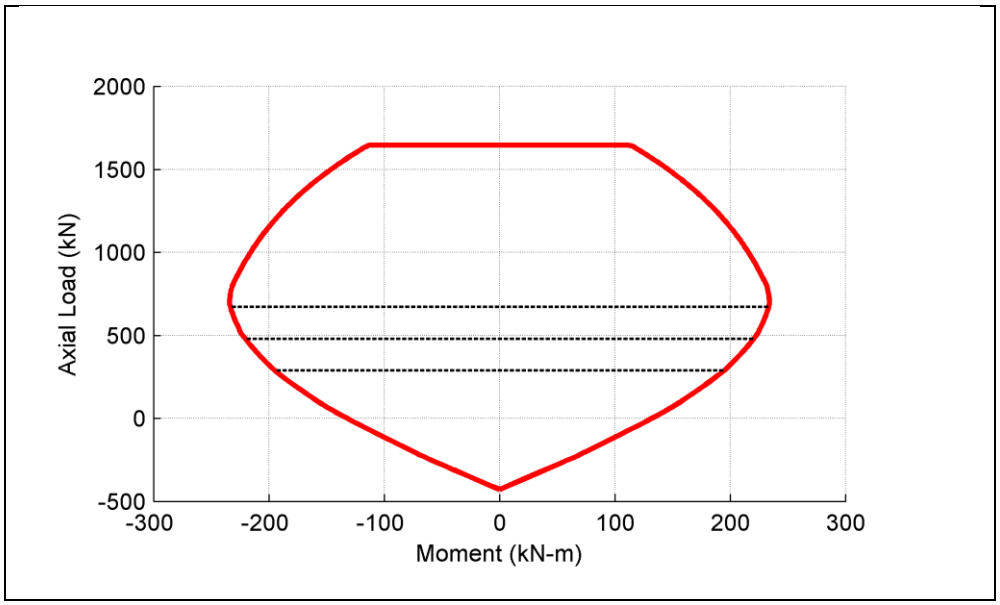

Figure 5.4. Nominal interaction curve of wall specimens according to ACI

From the interaction diagram (Figure 5.4), the nominal moment strength associated to an ALR of 0.15, 0.25, and 0.35 can be estimated. These moment strengths are summarized in Table 5.2 and the three levels of ALRs are shown with dashed lines in Figure 5.4. From the moment strength, the strenght of the specimens when subjected to lateral loads at the free end can be estimated considering a 175 cm wall height. These lateral strengths (fourth column of Table 5.2) are in average 50.2% smaller than the shear strength of the wall, therefore, the failure of this wall should be controlled by a flexural-compressive mode of failure.

Table 5.2. Moment and lateral strengths of wall specimens from ACI interaction diagram

ALR	**N (kN)**	**M_n (kN-m)**	**$V_{n\text{-}interaction}$ (kN)**
0.15	287.4	194.8	111.3
0.25	479.0	220.4	126.0
0.35	670.6	233.4	133.3

5.4 Moment – Curvature Relationships

The moment-curvature relationships under different ALRs were computed for the wall specimen cross section. A computational fiber-element model was developed in MATLAB (Mathworks, 2010) to conduct a section analysis of the wall specimen. Real strengths of the materials and the stress-strain relationships shown in sections 5.1 and 5.2 are considered in this analysis. The obtained moment-curvature relationships for ALRs of 0.15, 0.25 and 0.35 are shown in Figure 5.5. The figure shows that as the ALR increases, the moment strength increases, but the deformation capacity and ductility decrease. In the three cases shown in Figure 5.5, the failure of the wall section is controlled by the confined concrete compressive ultimate strain (ε_{cu} = 0.014) which is reached before the steel reaches its ultimate strain (ε_{su} = 0.166).

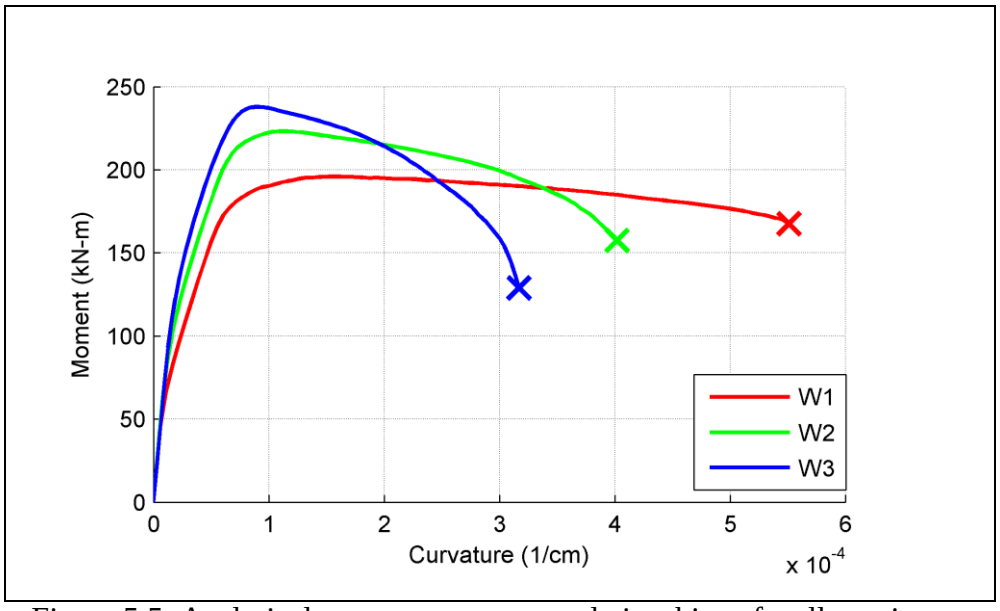

Figure 5.5. Analytical moment-curvature relationships of wall specimens

Considering the peak moment strengths from the moment-curvature relationships (Figure 5.5), the maximum lateral strengths of the wall specimens can be estimated. The predicted moment strength and the maximum lateral strengths are summarized in Table 5.3. The predicted lateral strengths of Table 5.3 are 0.5% to 2% higher than those obtained from the interaction curve (Table 5.2). The strength in both cases is similar because the strength of the core concrete is essentialy the same as the strength of the cover, which is the assumption used in ACI to obtain the interaction cruve.

Table 5.3. Moment and maximum lateral strengths of wall specimens from moment-curvature relationships

Specimen	**N (kN)**	**M_{max} (kN-m)**	**$V_{max\text{-}flex}$ (kN)**
W1	287.4	195.9	111.9
W2	479.0	223.3	127.6
W3	670.6	237.8	135.9

5.5 Displacement Estimation

Top horizontal yield and ultimate displacements for the wall were estimated using a plastic hinge approach (Figure 3.13(a)) based on the yield and ultimate curvatures obtained from the moment-curvature relations (Figure 5.5). A plastic hinge length of L_p = 2.5 t_w = 25 cm is assumed based on the tests results from Takahashi et al. (2013). The ACI318 (2011) approach (Figure 3.13(b)), which only includes plastic deformation was also considered for the estimation of the ultimate lateral displacement.

The yield curvature, ultimate curvature, and curvature ductility (φ_u/φ_y) for each ALR are listed in Table 5.4. The yield displacement, ultimate displacement and displacement ductility (δ_u/δ_y) for each ALR using the plastic hinge approach are listed in Table 5.5.

Table 5.4. Curvature and ductility estimation from moment-curvature relations

Specimen	φ_y **(1/cm)**	φ_u **(1/cm)**	φ_u/φ_y
W1	5.4E-05	5.5E-04	10.1
W2	6.1E-05	4.0E-04	6.6
W3	6.7E-05	3.2E-04	4.7

Table 5.5. Displacement (and % drift) and ductility estimation from plastic hinge approach

Specimen	δ_y **(mm)**	δ_u **(mm)**	δ_u/δ_y
W1	5.5 (0.3%)	25.7 (1.5%)	4.6
W2	6.2 (0.4%)	20.1 (1.1%)	3.2
W3	6.9 (0.4%)	17.0 (1.0%)	2.5

It can be concluded from Figure 5.5, Table 5.4 and Table 5.5 that high ALRs reduce significantly the wall ultimate curvature, displacement capacity, and ductility. For example, when the ALR is increased from 0.15 to 0.35, the ultimate curvature is reduced from 5.5E-04 to 3.2E-04 (58.2% reduction); the displacement capacity is reduced from 25.7 to 17 mm (33.9% reduction). This change in ALR also reduces the curvature ductility from 10.1 to 4.7 (53.5% reduction) and the displacement ductility from 4.6 to 2.5.

When the ACI318 (2011) approach is considered to estimate the ultimate lateral displacements 24.1, 17.5 and 14 mm are obtained for 0.15, 0.25 and 0.35 ALR respectively. These values are respectively 6.2%, 12.9 and 17.6% smaller than those from the plastic hinge model.

6. EXPERIMENTAL RESULTS

This section describes the observed damage and failure patterns of the three tested specimens. Load-displacement relationships, moment-curvature relationships, displacement capacities, peak strengths, top rotations and plastic hinge lengths were obtained for the wall specimens. Observations are made from the comparison between the three tests.

6.1 Observed Behavior

The behavior and failure of the three wall specimens with ALR of 0.15, 0.25 and 0.35 was controlled by axial-flexure interaction due to the relatively high M/Vl_w ratio of 2.5. The damage propagation and failure of W1, W2 and W3 are shown in Figure 6.1, Figure 6.2 and Figure 6.3, respectively. The crack initiation and propagation was similar for the three specimens at the first cycles of the tests. The first cracks were observed at 8.1 mm (0.5% drift) lateral displacement in the three specimens. These first cracks were diagonal shear cracks along the height of the walls which were followed by horizontal flexural cracks near the base of the walls on the tensile zone. The crack initiation is shown in figures Figure 6.1(a), Figure 6.2(a) and Figure 6.3(a) for specimen W1, W2 and W3, respectively.

The initiation of yielding occurred in the vertical boundary bars. Figure 6.4 and Figure 6.5 show the strains from strain gauges V1M and V7M which were located 20 cm above the concrete base in the boundary vertical bars V1 and V7, respectively (refer to Figure 4.11). For specimen W1, first yielding occurred in compression in bars V1 at a lateral displacement of 9.7 mm (0.6 % drift) and V7 bars also yielded in compression in the following loading reversal. For specimens W2 and W3 first yielding also occurred in compression in bars V1 at a lateral displacement of 4.9 mm (0.3% drift) and 4.6 mm (0.3% drift), respectively. Bars V7 also yielded in compression in the following cycle. In specimens W2 and W3 yielding occurred before the first observed crack. This early yielding in compression experienced by specimens W2 and W3 seems to be attributed to

the high compressive strain of about 0.001 (i.e. half of the yield strain of the steel bars) which was recorded after the application of the axial load. Figure 6.4 and Figure 6.5 also show a significant post-yielding strain increase in compression in strain gauges V1 and V7 in specimens W2 and W3 that may be attributed to bar buckling. This increase in compressive strain was not recorded immediately after yield initiation in specimen W1 possibly because reinforcement buckling did not occur at this early stage.

After reinforcement yielding, the horizontal flexural cracks (Figure 6.1(b) and Figure 6.2(b)) located near the base of the wall propagated towards the center of the wall specimens. Also, additional diagonal cracks were visible along the height of the wall in the three specimens. However, in specimen W3 these diagonal cracks were less and had lower thickness than those of W1 (Figure 6.1(b) and Figure 6.3(b)). Vertical cracks at the wall base in the position of bars V1 and V7 (Figure 6.2 (b)) were also visible after yielding, generally at a wall lateral displacement of 17.7 mm (1% drift), which seems to indicate that vertical reinforcement started to experiment bar buckling due to their high s/d_b = 9 ratio and started to push against the concrete cover (Figure 6.1(c), Figure 6.2(c) and Figure 6.3(c)). The complete spalling of concrete cover occurred at the wall edge generally at 26 mm displacement (1.5% drift) as shown in Figure 6.1(d). After reaching this drift level, specimen W3 with ALR of 0.35 failed immediately (Figure 6.3(d)) after concrete cover spalling at 26.5 mm displacement (1.5% drift). Specimen W2 with ALR of 0.25 survived longer and failed (Figure 6.2(d) and (e)) at the last reversal cycle of that same amplitude at -31.3 mm displacement (1.8% drift). On the other hand, specimen W1 with ALR of 0.15 could attain much more deformation after concrete cover spalling as its failure (Figure 6.1(e)) occurred at 48 mm displacement (2.8% drift). As shown in Figure 6.1(e), Figure 6.2(e) and Figure 6.3(d), not only the bars closest to the wall edge exhibited bar buckling; but also the second bars experimented buckling. Additionally, the horizontal reinforcement opened in the three specimens (Figure 6.6). This reinforcement opening was also observed in actual walls after the 2010 Chile earthquake and it is caused by the poor detailing with 90° hooks. Therefore, the low concrete confinement provided by the horizontal reinforcement became ineffective.

For the three specimens, the test ended when the walls were not able to carry the applied axial load. A brittle compressive failure along the entire length of the walls together with a sideway buckling was observed in the three specimens, as shown in Figure 6.1(f), Figure 6.2(f) and Figure 6.3(e). The observed failure mode of the three wall specimens was comparable to some damaged walls during the 2010 Chile Earthquake where crushing of concrete, buckling of vertical reinforcement and opening of horizontal reinforcement was observed (Figure 6.6).

The horizontal and vertical reinforcement bars in the three wall specimens did not experiment fracture during the tests. The fracture of vertical reinforcement in actual buildings may be attributed to additional cycles in damaged walls caused by the long duration of the earthquake. Since a constant vertical load was applied to the wall specimens, they were not able to transfer this load to adjacent structural elements and the specimens crushed in compression. The displacement cycles against time of each wall specimen are shown in Figure 6.7 and the observed behavior is highlighted in each specimen. The amplitude of the cycles corresponding to crack initiation, reinforcement yielding, vertical crack at the wall boundary, concrete cover spalling, and failure of each wall are summarized in Table 6.1. It is important to remark that high axial load triggered an early reinforcement yielding in compression for specimens W2 and W3 and reduced the deformation capacity from 48 mm in specimen W1 to 31.3 mm (34.8% reduction) and 26.5 mm (44.8% reduction) in specimens W2 and W3, respectively. It is apparent from Figure 6.7 that as the axial load increases, the “distance” between concrete cover spalling and brittle failure of the wall reduces drastically. This observation enables us to state that the observed failure in many walls during 2010 Chile Earthquake was brittle and occurred just a few cycles after cover concrete spalling. This is certainly inconsistent with the assumption of large strength reduction factors (R) in the design building codes.

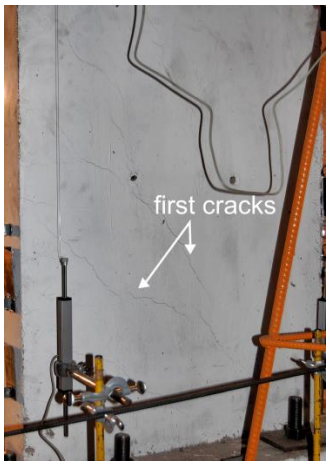

(a) First cracks

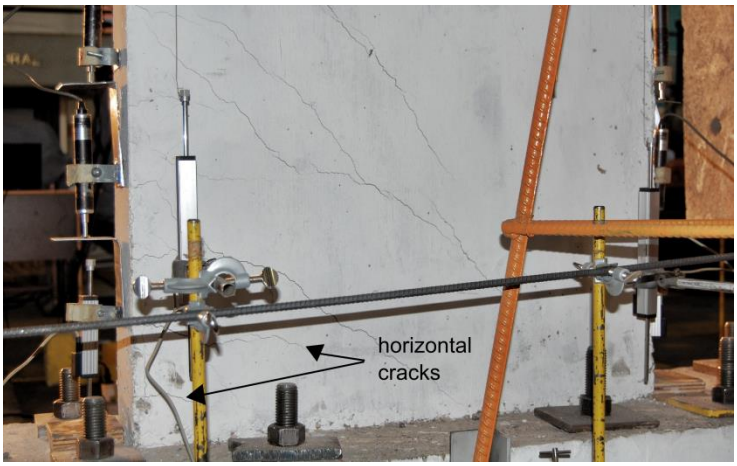

(b) Cracking development at δ=24.2 mm (1.4% drift)

(c) Initiation of cover concrete spalling

(d) Concrete spalling and bar buckling

(e) Concrete crushing failure

(f) Out-of-plane buckling

Figure 6.1. Specimen W1 observed behavior

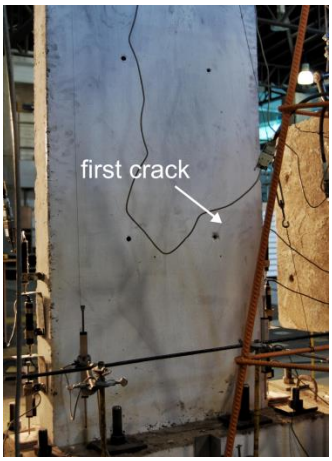

(a) First crack

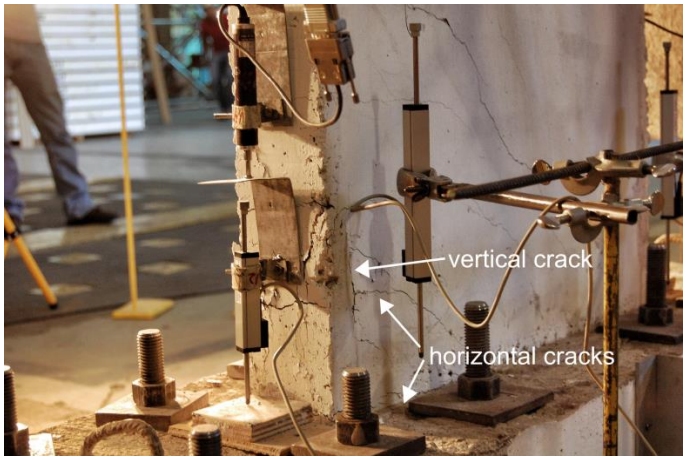

(b) Cracking development at δ=24.2 mm (1.4% drift)

(c) Cracking development at δ=31.3 mm (1.8% drift)

(d) Reinforcement buckling

(e) Concrete crushing failure

(f) Out-of-plane buckling

Figure 6.2. Specimen W2 observed behavior

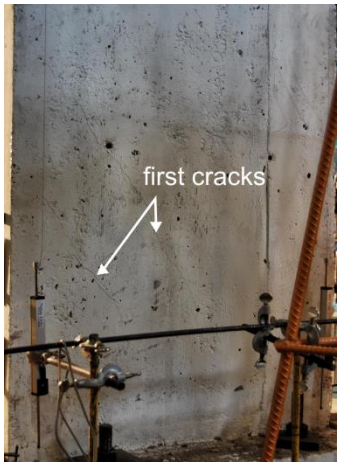

(a) First cracks

(b) Cracking development at δ=24.2 mm (1.4% drift)

(c) Initiation of cover concrete spalling

(d) Concrete crushing failure and bar buckling

(e) Out-of-plane buckling

Figure 6.3. Specimen W3 observed behavior

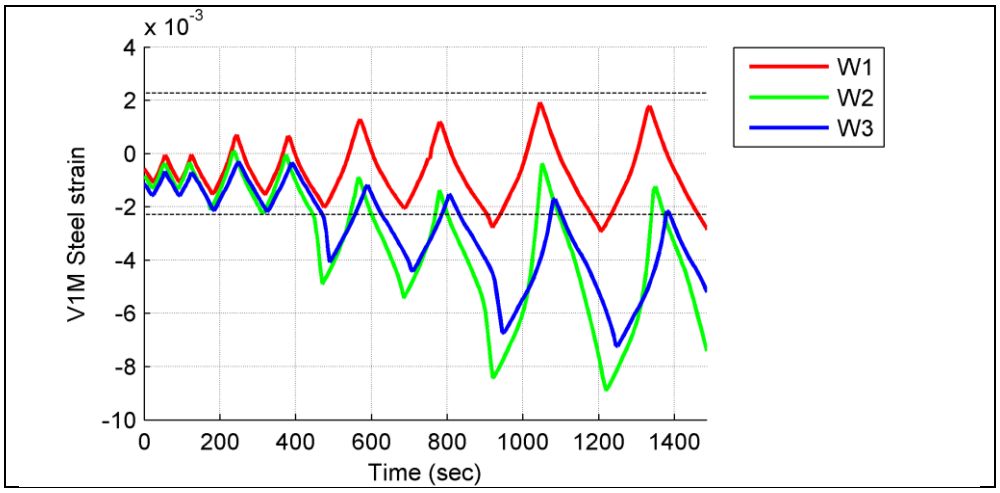

Figure 6.4. Strain versus time for strain gauge V1M for specimens W1, W2 and W3 (first four displacement amplitudes)

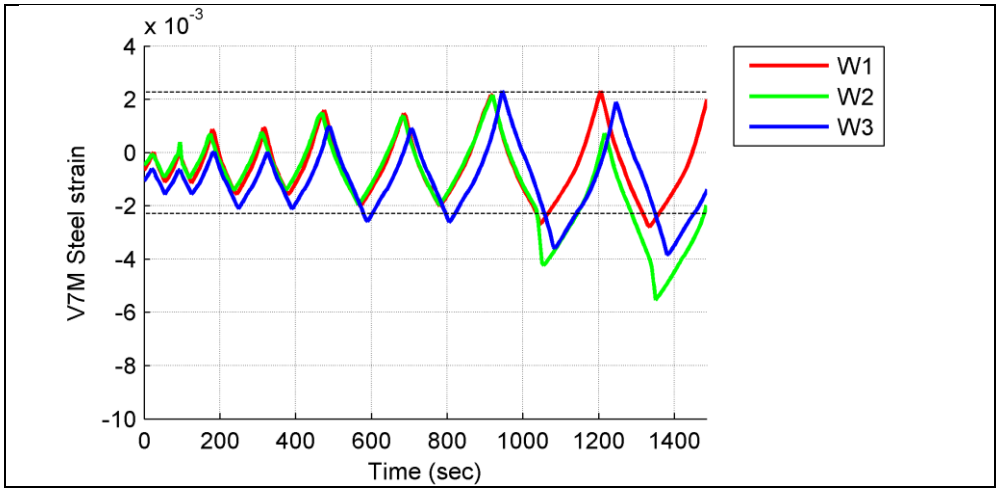

Figure 6.5. Strain versus time for strain gauge V7M for specimens W1, W2 and W3 (first four displacement amplitudes)

(a) W1 (b) W2 (c) W3 (d) 2010 Earthquake

Figure 6.6. Failure mode from the 2010 Chile Earthquake reproduced by the wall tests

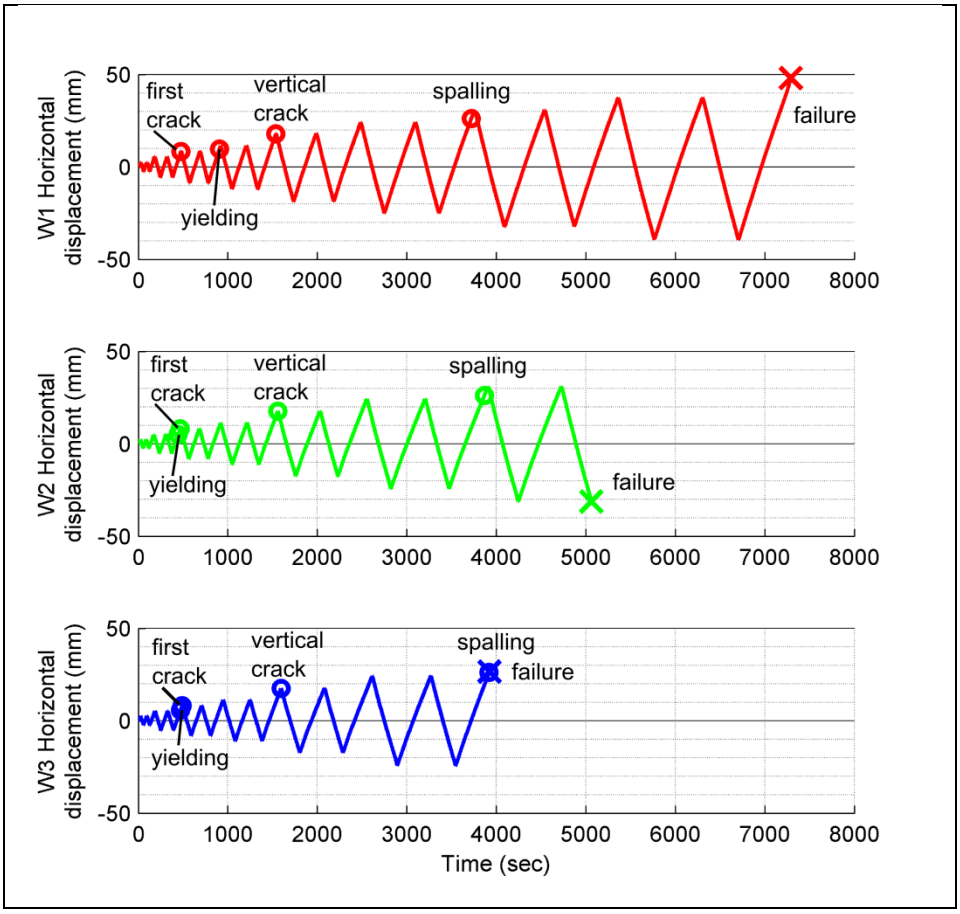

Figure 6.7. Wall displacements versus time and observed behavior of wall specimens

Table 6.1. Amplitude of cycles corresponding to observed behavior (mm)

Wall Specimen	**W1**	**W2**	**W3**
First observed crack	8.1	8.1	8.1
Reinforcement yielding	9.7	4.9	5.6
Vertical crack	17.7	17.7	17.7
Concrete spalling and reinforcement buckling	26.0	26.0	26.0
Concrete crushing failure	48.0	31.3	26.5

6.2 Vertical Load application

A constant ALR of 0.15, 0.25 and 0.35 was applied to specimens W1, W2 and W3 respectively. This axial load was controlled by keeping constant the oil pressure of the vertical actuator. Figure 6.8 shows the vertical load along time registered by the vertical load cell for the three wall specimens, which were not constant and some variations were recorded. A maximum increase of about 10% in the axial load was recorded when the wall reached peak displacements in both directions. This variation of the vertical load registered by the load cell seems to be attributed to the eccentricity in the load cell caused by the rotation of the top beam at peak displacements. These load variations were not observed in the oil pressure which had minimum variations during the test. Based on this argument, the vertical loads can be considered constant during the tests and equal to 287.4 kN, 478.7 kN and 671 kN for specimens W1, W2 and W3 respectively.

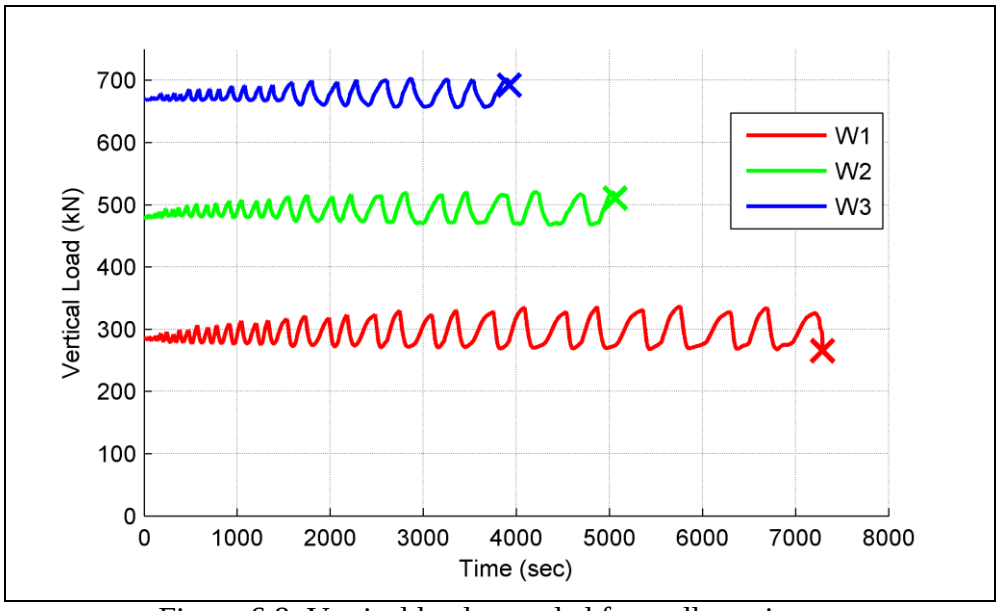

Figure 6.8. Vertical load recorded for wall specimens

6.3 Load-Displacement Relationships

The measured load-displacement relationships of specimens W1, W2 and W3 are shown in Figure 6.9, Figure 6.10 and Figure 6.11, respectively. The displacement was recorded using a displacement transducer located at the height of the actuator at the rear side of the wall specimens (refer to Channel 3 in Figure 4.10). For specimen W1, the peak lateral load of 144.3 kN was measured at 32.1 mm (1.8% drift), and reinforcement yielding initiated when the lateral load was 96.6 kN (67% of the peak load) at 9.7 mm peak displacement (0.6% drift). Specimen W1 failed under concrete crushing at 48 mm (2.8% drift) 7 cycles after reaching the peak strength. The ultimate lateral load recorded for specimen W1 was 81.3 kN (56.3% of the peak load). Figure 6.9 also shows an average strength reduction of 5.9% in the previous completed cycle of 39.3 mm (2.2% drift) amplitude. This strength reduction in subsequent cycles of equal amplitude is attributed to reinforcement buckling. For specimen W2 the measured peak load was 166 kN at 31.1 mm displacement (1.8% drift), and reinforcement yielding initiated at 73.4 kN (44.2% of the peak load) at 4.9 mm (0.3% drift). Specimen W2 experienced a

concrete crushing failure at a 31.3 mm displacement (1.8% drift) as shown in Figure 6.10. The failure occurred at the second reversed cycle and it was triggered by the strength reduction of 6.6% measured in the previous cycle of the same amplitude. The ultimate lateral load recorded for specimen W2 was 153.5 kN (92.4% of the peak). For specimen W3 (Figure 6.11) the measured peak lateral load was 185.6 kN at 21.44 mm displacement (1.2% drift), and reinforcement yielding initiated at 83.6 kN (45% of the peak load) at 5.6 mm (0.3% drift). A 6.7% average strength reduction was measured in the previous completed cycle at 24.4 mm displacement (1.39% drift). When vertical and horizontal cracks at the base of the wall were still developing in specimen W3, suddenly, the concrete reached high compression stresses which exceeded capacity and triggered a concrete crushing failure at 26.5 mm displacement (1.5% drift) with an ultimate strength of 146.5 kN (78.9 % of the peak).

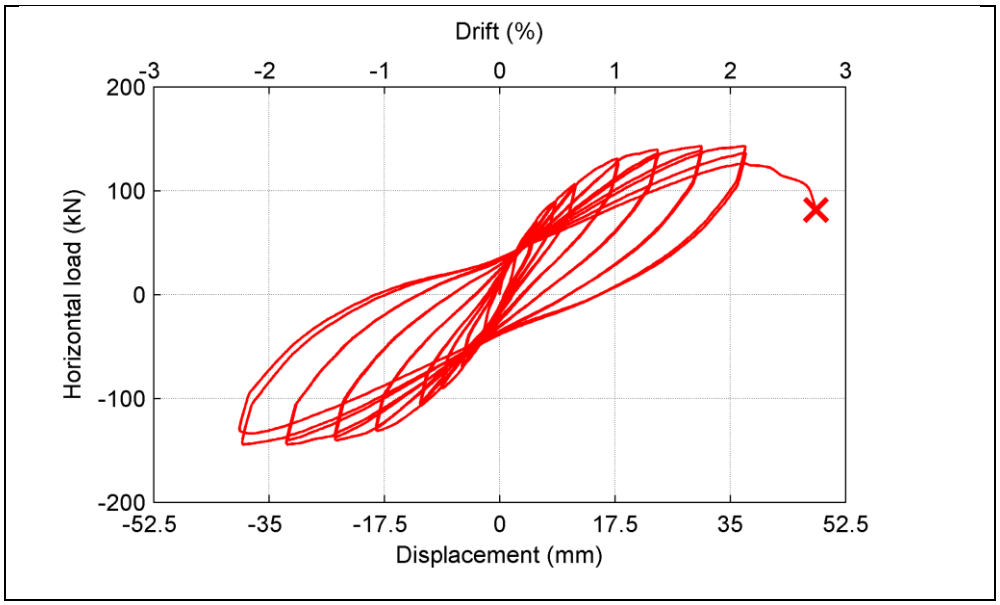

Figure 6.9. W1 load-displacement relationship

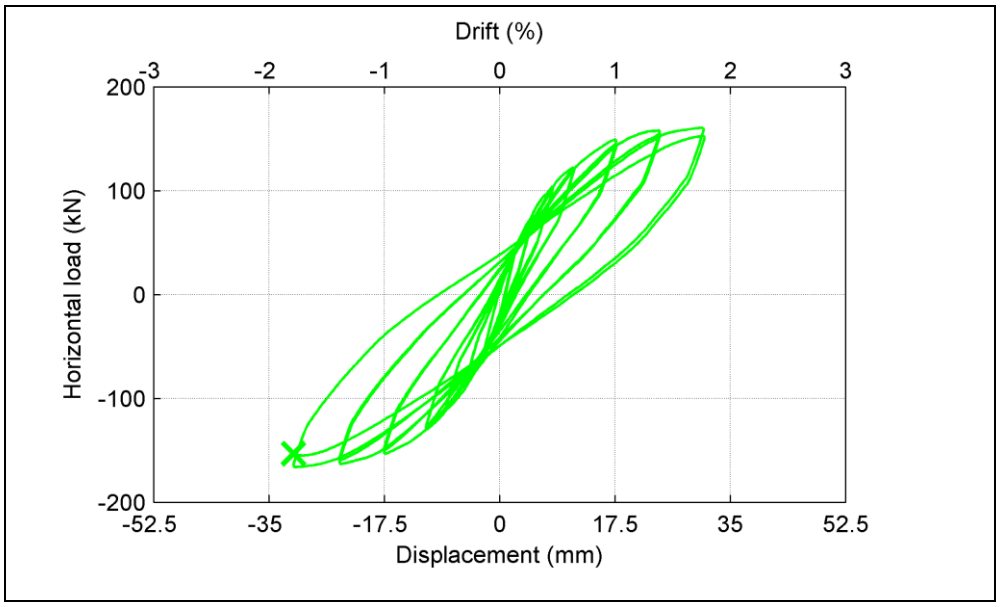

Figure 6.10. W2 load-displacement relationship

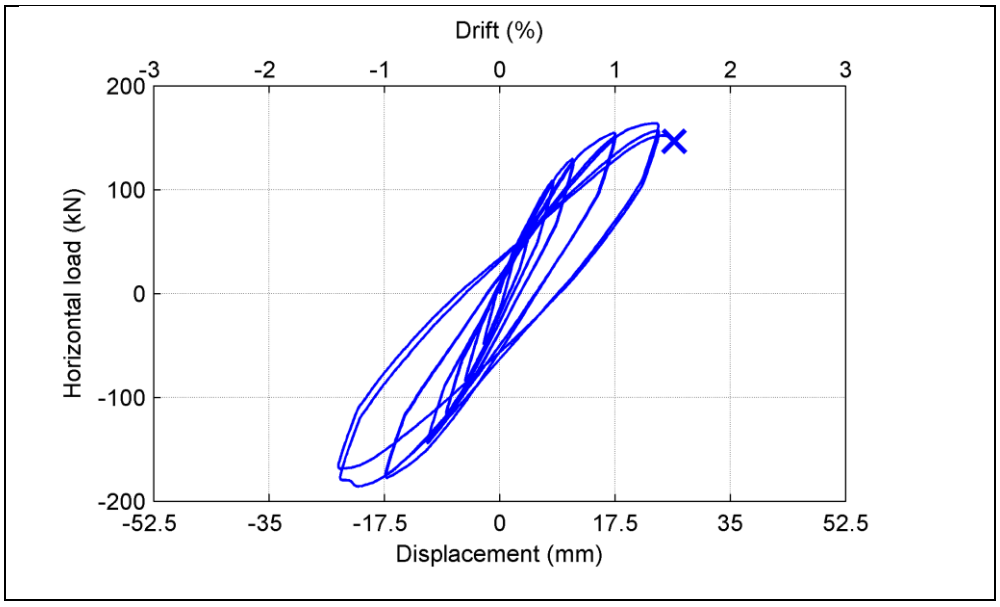

Figure 6.11. W3 load-displacement relationship

The three load-displacement relationships are shown together in Figure 6.12. The early reinforcement yielding and the displacement capacity reduction triggered by the relatively high ALRs were discussed in section 6.1. The lateral strength of the wall specimens (peak loads from the tests) are also influenced by the ALR. The 144.3 kN strength from specimen W1 increases to 166 kN (15% increase) and 185.6 kN (28.6%

increase) in specimens W2 and W3, respectively. However, the energy dissipated in the last completed cycle was 5.66 kN-m for W1, and 5.88 kN-m (13.9% reduction) and 3.67 kN-m (35.2% reduction) for specimens W2 and W3, respectively.

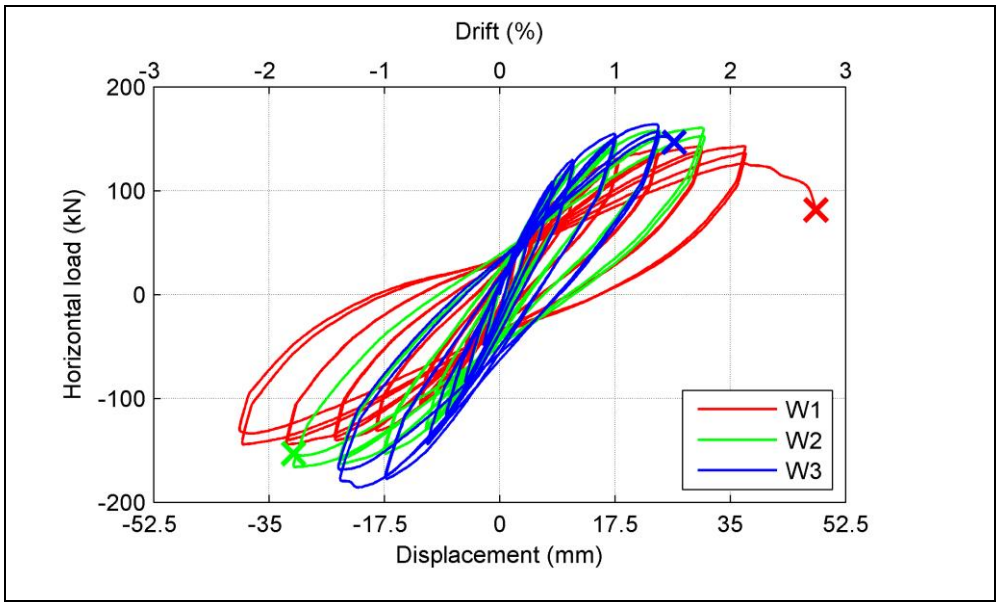

Figure 6.12. W1, W2 and W3 load-displacement relationships

6.4 Moment Curvature Relationships

The failure of the three wall specimens occurred near the bottom of the walls, at about 15 cm from the base. At that height, a displacement transducer was placed at both ends of the specimens in order to measure the vertical displacement of the wall edges with respect to the concrete base (Figure 4.10). Curvature was computed by subtracting those measures and dividing by the wall length of 70 cm. The moment at the critical section 15 cm above the concrete base was obtained by dividing the recorded lateral load by the 160 cm effective height at the critical section. The curvature was obtained until concrete cover spalling; after spalling, the displacement variations measured by the displacement transducer were inappropriate. However, peak moments and their corresponding curvatures were obtained for the three wall specimens. Yield moments and curvatures were also obtained from the points of the moment-curvature relations which correspond

to the time when the strain gauges measured yield strain (refer to Figure 6.4 and Figure 6.5). The moment curvature relationships obtained with the displacement transducers at the critical section for specimens W1, W2 and W3 are shown in Figure 6.13, Figure 6.14 and Figure 6.15, respectively.

For specimen W1 (Figure 6.13), the measured yield curvature is 1.43E-4 1/cm at a yield moment of 154.6 kN-m. The maximum moment is 230.9 kN-m at a curvature of 7.7E-04 1/cm. The yield curvature for specimen W2 (Figure 6.14) is 7.6E-05 1/cm at a yield moment of 117.4 kN-m, and the maximum moment is 265.6 kN-m at a curvature of 3.8E-04. For specimen W3 (Figure 6.15) the yield curvature is 8.9E-05 1/cm at a yield moment of 133.8 kN-m moment, and the maximum moment is 297 kN-m at a curvature of 4.3E-04 1/cm. This latter specimen showed a brittle failure which occurred almost at the same time of concrete cover spalling. Hence, for specimen W3, it was possible to measure the ultimate curvature accurately which is 6.5E-04 1/cm at 234.4 kN-m moment. The effects of the ALR in the moment-curvature relationships is similar than the effects in the load-displacement relationships; W2 and W3 exhibited an early yield curvature (around 50% reduction than the W1 yield curvature) and the peak moment strengths in the critical section of W2 and W3 are respectively 15% and 28.6% higher than the peak moment strength in W1.

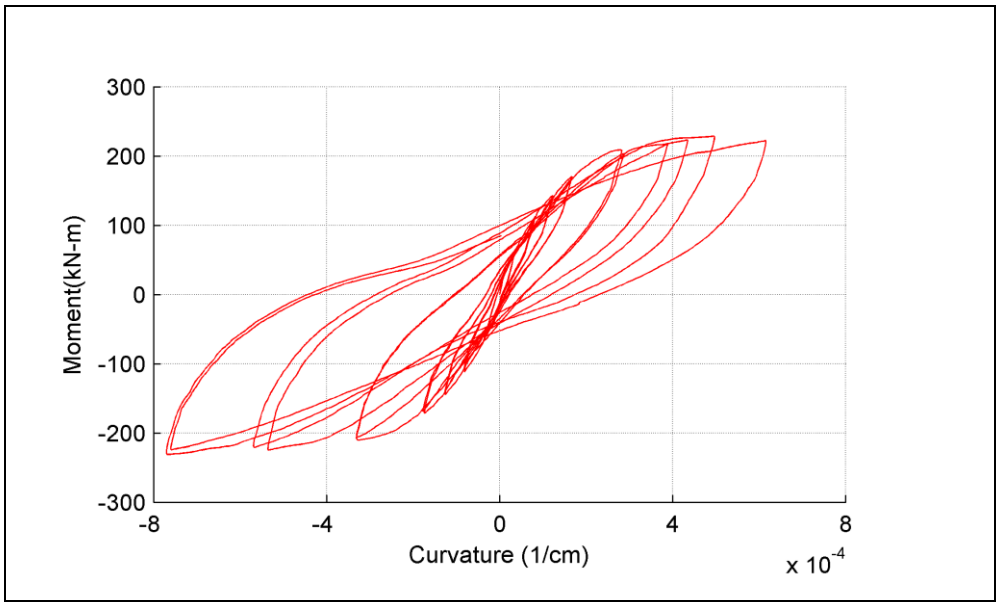

Figure 6.13. W1 Moment-curvature relationship

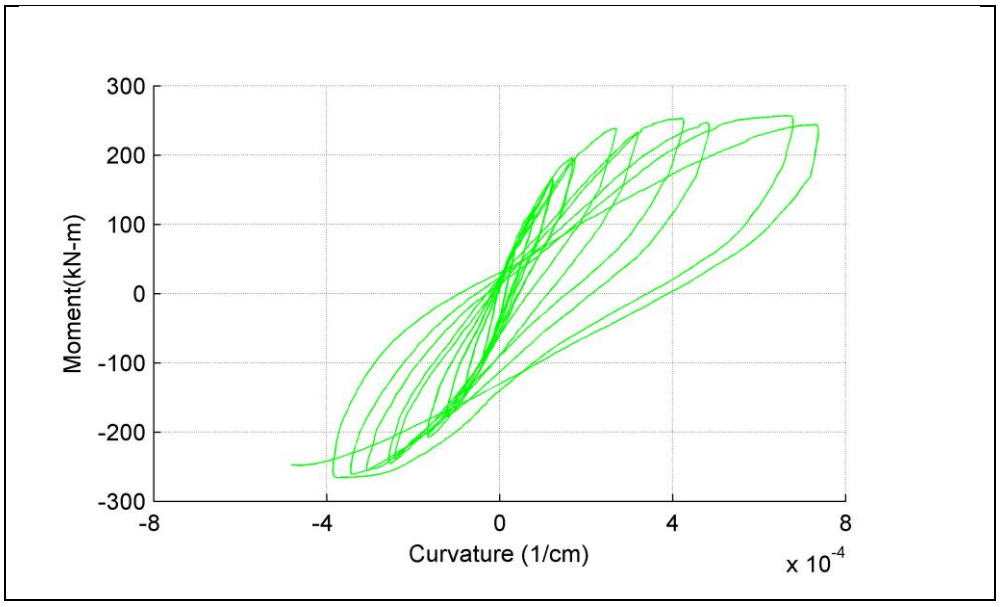

Figure 6.14. W2 Moment-curvature relationship

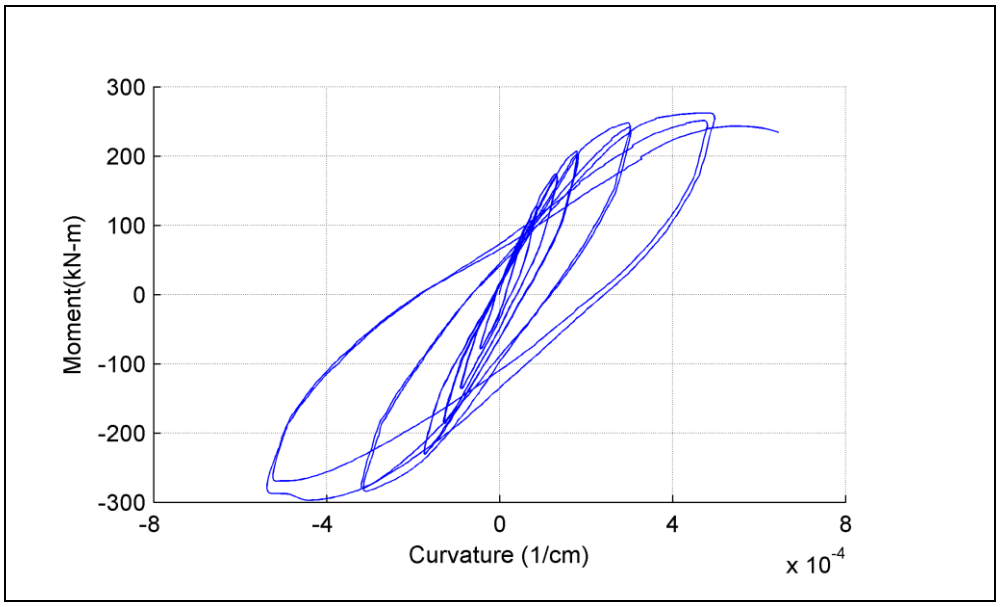

Figure 6.15. W3 Moment-curvature relationship

6.5 Top Rotation

The top rotation of the three wall specimens was obtained during the tests. Two displacement transducers were attached to the top concrete beam at 5 cm of both wall ends (refer to channels 7 and 8 in Figure 4.10) in order to measure the vertical displacement of the wall edges. The rotation was computed by subtracting those displacements and dividing by the distance between the transducers of 60 cm. The top rotation versus time for specimens W1, W2 and W3 are shown in Figure 6.16. The ultimate recorded rotation was 0.028, 0.018 and 0.016 rad for specimens W1, W2 and W3, respectively.

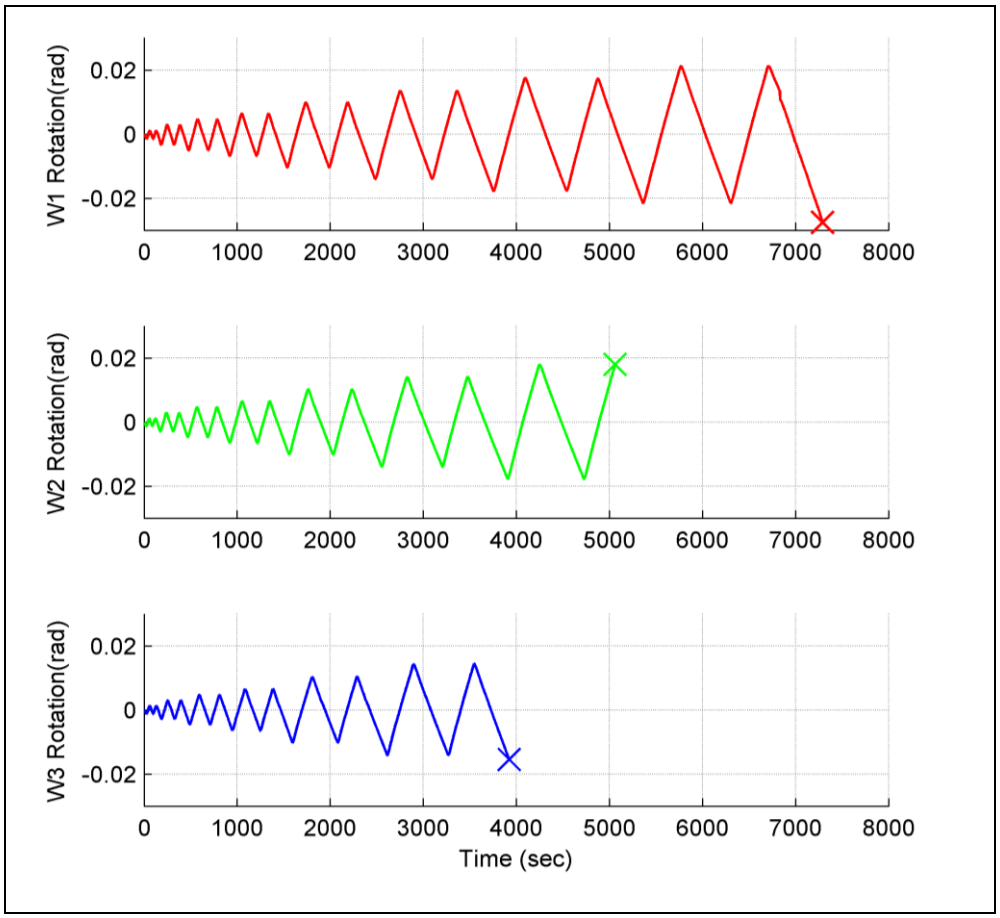

Figure 6.16. Top rotation versus time for wall specimens

6.6 Plastic Hinge Length

The damage in the three wall specimens was concentrated at the bottom of the wall, near the concrete base (Figure 6.17). This area is referred to as the plastic hinge zone. The measured plastic hinge length for the three tests which is considered as the length from the concrete base to the zone where concrete cover did not spall. The average plastic lengths measured along the wall length for W1, W2 and W3 are 22, 24 and 27 cm, respectively.

(a) W1 (b) W2 (c) W3

Figure 6.17. Damage concentration at the bottom of wall specimens

7. ANALYTICAL-EXPERIMENTAL COMPARISON

The experimental wall strengths, yield displacements and ultimate displacements from Chapter 6 are compared in this Chapter with the predictions from the analytical pre-test analysis performed in Chapter 5. The wall plastic hinge length is also discussed in this Chapter.

7.1 Wall Strength

The peak lateral strength obtained from the three tests (refer to section 6.3), and the analytical strength obtained from the flexural and shear analysis performed in section 5.4 are compared in Table 7.1. The three experimental strengths were in average 33.4% lower than the shear strength, hence, the behavior was controlled by flexure. However, the experimental strengths were in average 21.4% larger than the analytical strengths obtained from the flexural analysis.

Table 7.1. Analytical and experimental lateral strength of wall specimens

Specimen	**V_{shear} (kN)**	**V_{flex} (kN)**	**$V_{experimental}$ (kN)**	**Difference (%)**
W1	248.3	111.9	144.3	22.5%
W2	248.3	127.6	166.0	23.1%
W3	248.3	135.9	185.6	26.8%

As discussed in section 6.4, the critical section of the wall was not at the concrete base. The critical section where a plastic hinge occurred was about 15 cm above the concrete base. Therefore, a 160 cm effective wall height may be considered for the analytical strength using flexural analysis instead of the 175 wall cm height considered in Chapter 5. If the 160 cm effective wall height is considered, the analytical lateral strength for specimens W1, W2 and W3 are on average 17% larger than the experimental results, as

shown in Table 7.2. This difference is acceptable and seems to be attributed to the fact that the wall thickness of the tests specimens ranged between 10.5 and 10.8 cm instead of the 10 cm thickness considered in the analytical estimations, which increases the wall strength. The differente may also be attributed to some confinement of concrete that mat have been present in the rectangular wall cross section which could have increased the concrete strength in comparison with the cylindrical samples.

Table 7.2**.** Analytical (effective 160 cm wall height) and experimental wall strength

Specimen	**V_{shear} (kN)**	**V_{flex} (kN)**	**$V_{experimental}$ (kN)**	**Difference (%)**
W1	248.3	122.4	144.3	15.2%
W2	248.3	139.6	166.0	15.9%
W3	248.3	148.6	185.6	19.9%

7.2 Yield and ultimate displacement

The estimated yield displacement obtained from the moment-curvature relationships and the plastic hinge approach in section 5.5 is compared with the experimental yield displacement (section 6.1). This comparison is shown in Table 7.3 where relatively high errors are obtained. It is important to note that the experimental yield displacement was related to the time when the first strain gauge yielded, which may be later than the actual yielding of the bar in a different location. However, the analytical prediction considers only the flexural behavior and other effects should be considered for the tested wall specimens; reinforcement slip of vertical bars, shear deformations and the rigid body rotation experimented by the wall specimens.

Table 7.3. Analytical and experimental yield displacement

Specimen	**$\delta_{y\text{-}flex}$(mm)**	**$\delta_{y\text{-}experimental}$ (mm)**	**Difference (%)**
W1	5.5	9.7	43.3%
W2	6.2	4.9	-26.5%
W3	6.9	5.6	-23.2%

According to Sezen and Setzler (2008), reinforcement slip due to strain accumulation in steel bars subjected to tension may produce considerably large deformations in a RC structural member subjected to lateral loads. The horizontal displacement contribution of slip deformation estimated by the model shown in Figure 7.1 is considered in this analysis to estimate the specimens yield displacement. The slip deformation at the base-wall interface of the vertical bars is obtained from:

$$slip = \begin{cases} \frac{\varepsilon_s l_d}{2} & for\ \varepsilon_s \leq \varepsilon_y \\ \frac{\varepsilon_y l_d}{2} + \frac{(\varepsilon_s + \varepsilon_y) l'_d}{2} & for\ \varepsilon_s > \varepsilon_y \end{cases} \quad (9)$$

Where ε_s and ε_y are the tensile strain and the yield strain of the steel bar respectively; l_d and l'_d are the bar development lengths for elastic and inelastic ranges respectively, which are defined as:

$$l_d = f_s d_b / 4u_b \quad (10)$$

$$l'_d = \frac{(f_s - f_y) d_b}{4u'_b} \quad (11)$$

Where f_s and f_y are the tensile stress and yield stress of the steel bar respectively; d_b is the bar diameter; and $u_b = 1.0\sqrt{f'_c}\,MPa$ and $u'_b = 0.5\sqrt{f'_c}\,MPa$ are the bond stress

capacities before and after yielding. Then, the lateral displacement of the wall due to reinforcement slip is estimated considering a rigid frame rotation of the body as:

$$\delta_s = \theta_s h = \frac{slip}{d-c}\, h \tag{12}$$

Where *d* is the wall length measured from the bar position (68 cm), *c* is the neutral axis depth at yield moment which is obtained from the flexural analysis performed in section 5.4, and *h* is the height of the cantilever wall (175 cm).

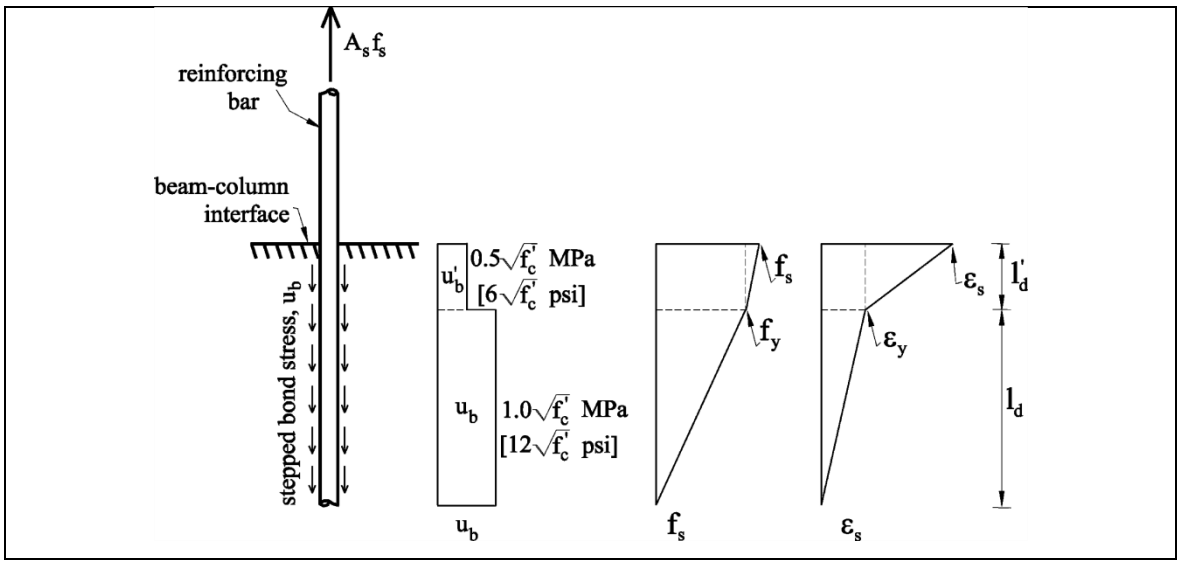

Figure 7.1. Reinforcement Slip Model (Sezen & Setzler, 2008)

Elastic shear deformations of the specimens are taken into account. At yielding, the lateral displacements induced by shear deformation are computed as:

$$\delta_{sh} = \frac{V_y\, l}{G A_{sh}} \tag{13}$$

Where V_y is the analytical lateral strength from Table 7.2, l=1.6 m is the effective height of the wall, $G = E/2(1+v)$ = 10900 MPa is the shear modulus of elasticity, v is the Poisson's ratio considered as 0.2 for concrete, and $A_{sh} = A/1.2 = 583.3\ cm^2$ is the effective shear area.

Also, the eventual rotation of the RC base of the wall specimens is considered. The vertical displacement of the base at the edge of the wall was measured in the experiments by a displacement transducer (refer to channel 16 in Figure 4.10) and its contribution to the lateral displacement of the wall can be obtained assuming a rigid body rotation of the RC wall base. If the reinforcement slip, the shear deformation and the rigid body rotation of the RC wall are considered, the yield displacements for the three wall specimens are obtained from equation (14) and are shown in Table 7.4:

$$\delta_{y-analytical} = \delta_{y-flex} + \delta_{y-slip} + \delta_{y-shear} + \delta_{y-rot} \quad (14)$$

Table 7.4. Analytical contribution to yield displacement and experimental yield displacement

Specimen	**$\delta_{y\text{-}flex}$ (mm)**	**$\delta_{y\text{-}slip}$ (mm)**	**$\delta_{y\text{-}shear}$ (mm)**	**$\delta_{y\text{-}rot}$ (mm)**	**$\delta_{y\text{-}analytical}$ (mm)**	**$\delta_{y\text{-}experimental}$ (mm)**	**Difference (%)**
W1	5.5	0.9	0.3	0.8	7.5	9.7	22.7%
W2	6.2	1.1	0.4	0.6	8.3	4.9	-69.4%
W3	6.9	1.2	0.4	0.6	9.1	5.6	-62.5%

From Table 7.4 it can be concluded that the yield displacement was not predicted accurately for the tested walls. For specimens W2 and W3, the early yield in compression experienced by the vertical reinforcement bars was not predicted by the analytical model. For specimen W1 the displacement prediction of the analytical model was somehow better, and it underestimated the experimental yield displacement by 23%. The moment-curvature analysis, plus the consideration of other effects involved in the displacement was not capable to predict an accurate yielding displacement for these wall specimens and probably a more complex finite element analysis should be performed for

a better prediction, or the walls should have been instrumented with additional strain gauges to obtain a more reliable experimental yield strain.

The ultimate displacement estimated with the plastic hinge approach with a plastic hinge length of L_p = 2.5 t_w = 25 cm (section 5.5) is compared with the experimental ultimate displacement (section 6.1). This comparison is shown in Table 7.5 where the experimental displacement is on average 39% larger than the analytical displacement.

Table 7.5. Analytical and experimental ultimate displacement

Specimen	**$\delta_{u\text{-}flex}$ (mm)**	**$\delta_{u\text{-}experimental}$ (mm)**	**Difference (%)**
W1	25.7	48.0	46.5%
W2	20.1	31.3	35.8%
W3	17.0	26.5	35.8%

If the displacement induced by reinforcement slip and the rigid body rotation is included (the shear effects were neglected at ultimate level), the ultimate displacements for the three wall specimens are obtained from equation (15). These displacements and are shown in Table 7.6.

$$\delta_{u-analytical} = \delta_{u-flex} + \delta_{u-slip} + \delta_{u-rot} \quad (15)$$

Table 7.6. Analytical contribution to ultimate displacement and experimental ultimate displacement

Specimen	$\delta_{u\text{-}flex}$ (mm)	$\delta_{u\text{-}slip}$ (mm)	$\delta_{u\text{-}rot}$ (mm)	$\delta_{u\text{-}analytical}$ (mm)	$\delta_{u\text{-}experimental}$ (mm)	Error (%)
W1	25.7	14.1	1.7	41.5	48.0	13.5%
W2	20.1	8.2	1.6	29.9	31.3	4.5%
W3	17.0	6.2	1.6	24.8	26.5	6.4%

The underestimation of the ultimate displacement of 8.1% in average by the analytical model is acceptable. The plastic hinge approach using the curvature from the flexural analysis and considering a plastic hinge length of L_p = 2.5 t_w = 25 cm is adequate to estimate the ultimate displacements when the effects of reinforcement slip and rigid body rotation of the RC base are added. This plastic hinge length is also consistent with the measured plastic hinge length from section 6.6.

7.3 Ultimate Top Rotation

The comparison between the experimental ultimate top rotation of the three wall specimens and the analytical estimation are shown in Table 7.7. The measured top rotations of the walls are shown in Figure 6.16. The analytical estimation of the top rotation is obtained from the plastic hinge approach (Figure 3.13 (a)), where the ultimate rotation θ_u is estimated from the curvatures obtained from the flexural analysis (section 5.4) using equation (16), where a plastic hinge of L_p = 2.5 t_w = 25 cm is considered:

$$\theta_u = \frac{\varphi_y L}{2} + (\varphi_u - \varphi_y) L_p \tag{16}$$

Table 7.7. Analytical and experimental ultimate top rotation

Specimen	**$\theta_{u\text{-}flex}$ (rad)**	**$\theta_{u\text{-}experimental}$ (rad)**	**Difference (%)**
W1	0.017	0.028	37.8%
W2	0.014	0.018	22.7%
W3	0.012	0.016	21.7%

Table 7.7 shows that the experimental rotation is on average 27.4% larger than the analytical rotation. If the rotations induced by the reinforcement slip and by the rigid body rotation of the RC base are added (which are obtained dividing the corresponding displacement from Table 7.6 by the 1750 mm wall height) the ultimate top rotation for the three wall specimens are obtained from equation (17) and are shown in Table 7.8.

$$\theta_u(Analytical) = \theta_{flex} + \theta_{slip} + \theta_{rot} \tag{17}$$

Table 7.8. Analytical contribution to ultimate top rotation and experimental ultimate top rotation

Specimen	**$\theta_{u\text{-}flex}$ (rad)**	**$\theta_{u\text{-}slip}$ (rad)**	**$\theta_{u\text{-}rot}$ (rad)**	**$\theta_{u\text{-}analytical}$ (rad)**	**$\theta_{u\text{-}experimental}$ (rad)**	**Difference (%)**
W1	0.0172	0.0081	0.0010	0.0262	0.0276	5.1%
W2	0.0138	0.0047	0.0009	0.0194	0.0179	-8.6%
W3	0.0121	0.0035	0.0009	0.0166	0.0155	-7.0%

Table 7.8 shows that the analytical ultimate rotations using equation (17) overestimate the experimental rotation on average by 3.5%, which is considered adequate. The plastic hinge approach using the yield and ultimate curvature from the flexural analysis and considering a plastic hinge length of L_p = 2.5 t_w = 25 cm is adequate to estimate the ultimate top rotation when the effects of the reinforcement slip and the rigid body rotation of the RC base are added. This plastic hinge length is also consistent with the measured plastic hinge length from section 6.6 and the ultimate displacement estimation from section 7.2.

8. CONCLUSIONS

The M_w=8.8 Earthquake that struck southern and central Chile in 2010 provides valuable information about building performance. Despite of the global assessment of acceptable performance of RC buildings, the observed brittle damage induced by the earthquake motivates conducting research with the purpose of improving the seismic design provisions of RC buildings.

The characteristics of critical walls in five damaged buildings were obtained from a survey performed in this research. The average M/Vl_w ratio was 2.02, which implies that flexural behavior was relevant. Wall thicknesses varied from 15 cm to 25 cm, which seems to be relatively low. This low wall thickness plus the increase in building heights lead to a considerable increase in axial loads in RC walls of newer buildings compared to buildings before 1985 Chile Earthquake. The average ALR of the walls was 0.38 for ultimate loads, where 37% of the surveyed walls had ALR larger than 0.35, which is the limit imposed by the Chilean code after 2010 earthquake. During 2010 Earthquake, RC walls were subjected to high axial loads which made them susceptible to brittle compression controlled behavior. RC walls were provided with large vertical reinforcement ratios to provide strength but with inadequate transverse reinforcement. A detailed analysis of one damaged wall in a buildings located in Concepción was performed in order to understand the observed failure. The high ALR, the inadequate concrete confinement, and the lack of restrain for longitudinal bar buckling (s/d_b ratio of 16.7) compromised the displacement capacity of the wall and a brittle flexural-compressive failure mode was generated. The provided wall ductility was not consistent with the load reduction factor (R*) of 6.42 considered in the design of such building.

Three identical ½-scale wall specimens (W1, W2 and W3) were designed with representative characteristics that were obtained from the described survey. These wall specimens were tested in order to reproduce and understand the observed damage in walls during the 2010 Earthquake. The wall specimens were subjected to equal double-

cycle lateral displacements for each wall specimen and constant ALRs of 0.15, 0.25 and 0.35 for W1, W2 and W3, respectively. The following findings were obtained from the test results and analytical calculations:

- The flexural-compressive failure mode observed in RC walls during 2010 Chile Earthquake was reproduced experimentally in this research. Concrete crushing, vertical reinforcement buckling and horizontal reinforcement opening at wall boundaries observed in the tests was similar to the observed damage in walls during the earthquake. The wall specimens showed out-of-plane wall buckling which was induced by the compressive failure and low wall thickness. This out-of-plane buckling was also observed in damaged walls during the earthquake. The failure mode of specimen W3, under relatively high ALR of 0.35, was brittle and extremely sudden; concrete crushing in compression occurred immediately after cover concrete spalling. Specimen W2, with ALR of 0.25, showed the same type of failure mode but less brittle because failure occurred three cycles after cover concrete spalling. For specimen W1, with relatively low ALR of 0.15, the behavior was more ductile than that of the other two wall specimens; it resisted seven displacement cycles between cover concrete spalling and concrete crushing failure.
- Displacement capacity is reduced significantly as ALR increases. The ultimate displacement for specimens W2 and W3 were 34.8% and 44.8% smaller than that from specimen W1. Therefore, the displacement capacity was reduced almost the half when the ALR was increased from 0.15 to 0.35. The measured ultimate drift of specimens W1, W2 and W3 was 2.7%, 1.8% and 1.5%, respectively.
- The wall lateral strength increases as ALR increases. The peak lateral load for specimens W2 and W3 were 15% and 28.6% higher than that from specimen W1.
- High ALRs triggered a compressive reinforcement yielding in the three specimens which was not predicted by the analytical models. In case of

specimens W2 and W3, yielding occurred earlier than in specimen W1; even before the first visible crack.

- The average measured plastic hinge length for the three specimens was 24.3 cm which is about 2.5 times the wall thickness. This observation agrees well with the result obtained by Takahashi et al (2013). The simplified plastic hinge approach with a plastic hinge length of $L_p = 2.5\ t_w$ including the rigid body displacement due to reinforcement slip and base rotation of the RC base estimates adequately the ultimate wall displacements and top rotations.
- The ALR limit of 0.35 for ultimate axial loads imposed in DS 60 (2011) is not adequate for thin unconfined RC walls, since the provided displacement capacity and ductility are not consistent with the strength reduction factor of the design code. However, DS 60 (2011) improves wall design. It provides guidelines to verify if a wall requires special boundary confinement, with a similar approach than that from ACI, and it requires a minimum wall thickness of 30 cm when a wall requires confinement. Hence, these provisions should increase wall displacement capacity in newer buildings.

The research project which involves this thesis includes eight additional wall tests which are aimed to study other wall characteristics such as wall thickness, M/Vl_w ratio and reinforcement detailing. For future research it is strongly recommended to test RC walls built with special boundary confinement to validate the ALR limit of 0.35 adopted by the current Chilean code. Additionally, some buildings which did not exhibit damage in 2010 may be susceptible to the studied brittle behavior in a future earthquake. These structures should be analyzed in order to determine if retrofit is required to sustain several inelastic deformation cycles in future events. The use of energy dissipation devices in such buildings may be a good alternative for retrofitting since they could limit the flexural-compressive failure mode exhibited by the wall buildings and the tested specimens. Finally, a similar experimental project should be performed in order to analyze the behavior of T (or other shape) walls which are common in Chilean residential buildings and that exhibited brittle damage after the 2010 Earthquake. As an

experimental project involving this type of walls may be difficult to conduct at Pontificia Universidad Católica with the available equipment, nonlinear finite-element analysis could be a good alternative to study the behavior of such RC walls. The finite element model could be calibrated, at least for rectangular walls, with the test results obtained from this experimental project.

REFERENCES

American Concrete Institute (ACI). (1995). *Building Code Requirements for Structural Concrete and Commentary (ACI 318-95).*

American Concrete Institute (ACI). (2005). *Building Code Requirements for Structural Concrete and Commentary (ACI 318-05).*

American Concrete Institute (ACI). (2008). *Building Code Requirements for Structural Concrete and Commentary (ACI 318-08).*

American Concrete Institute (ACI). (2011). *Building Code Requirements for Structural Concrete and Commentary (ACI 318-11).*

Canadian Standards Association. (2004). *Design of Concrete Structures for Buildings (CSA A23.3-04)*. Toronto.

China Ministry of Construction. (2010). *Code for Seismic Design of Buildings (GB 50011-2010)*. Beijing, China.

Computers & Structures, Inc. (2011). ETABS v.9.7.1. Berkeley, California, USA.

Decreto número 60 (DS 60). (2011). *Requisitos de Diseño y Cálculo para el Hormigón Armado.* Diario Oficial de la República de Chile.

Decreto número 61 (DS 61). (2011). *Diseño Sísmico de Edificios.* Diario Oficial de la República de Chile.

EERI. (2010, June). The Mw 8.8 Chile Earthquake of February 27, 2010. *EERI Earthquake Special Report*.

European Comittee for Standardization. (2004). *European Standard EN1998-1 Eurocode 8: Design of Structures for Earthquake Resistance - Part 1: General Rules, Seismic Actions and Rules for Buildings.* Brussels.

Gobierno del Distrito Federal. (2004). *Normas Técnicas Complementarias para Diseño y Construcción de Estructuras de Concreto (NTCC-04).* México D.F.: Gaceta Oficial del Distrito Federal, Tomo I, No. 103 bis.

Hidalgo, P. A., Ledezma, C. A., & Jordán, R. M. (2002). Seismic behavior of Squat Reinforced Concrete Shear Walls. *Earthquake Spectra 18(2)*, 187-208.

Instituto Nacional de Normalización (INN). (1996). *Diseño Sísmico de Edificios, (NCh433 Of.1996).* Santiago, Chile.

Instituto Nacional de Normalización (INN). (2008). *Hormigón Armado - Requisitos de Diseño y Cálculo, NCh430Of.2008.* Santiago, Chile.

Instituto Nacional de Normalización (INN). (2009). *Diseño Sísmico de Edificios, (NCh433 Of.1996 Mod 2009).* Santiago, Chile.

Instituto Nacional de Normalización (INN). (2010). *Diseño estructural - Disposiciones generales y combinaciones de cargas.* Santiago, Chile.

International Conference of Building Officials. (1997). *Uniform Building Code (UBC97).* Whittier, CA.

Jünemann, R., Hube, M., De La Llera, J. C., & Kausel, E. (2012). Characteristics of Reinforced Concrete Shear Wall Buildings Damaged During 2010 Chile Earthquake. *15 WCEE*. Lisboa.

Karthik, M., & Mander, J. (2011). Stress-Block Parameters for Unconfined and Confined Concrete Based on a Unified Stress-Strain Model. *Journal of Structural Engineering 137(2)*, 270-273.

Mander, J., Priestley, M., & Park, R. (1988). Theoretical Stress-Strain Model for Confined Concrete. *Journal of Structural Engineering 114(8)*, 1804-1826.

Massone, L., Bonelli, P., Lagos, R., Lüders, C., Moehle, J., & Wallace, J. (2012). Seismic Design and Construction Practices for RC Structural Wall Buildings. *Earthquake Spectra 28(S1)*, S245-S256.

MathWorks Inc. (2010). *MATLAB version R2010b.*

Monti, G., & Nuti, C. (1992). Nonlinear Cyclic Behavior of Reinforcing Bars Including Buckling. *Journal of Structural Engineering, 118(12)*, 3268-3284.

Riddell, R., Wood, S. L., & De la Llera, J. C. (1987). The 1985 Chile Earthquake: Structural Characteristics and Damage Statistics for the Building Inventory in Viña del Mar. *Civil Engineering Studies, Structural Research Series No. 534, Univeristy of Illinois, Urbana*.

Rodriguez, M., Botero, J., & Villa, J. (1999). Cyclic Stress-Strain Behavior of Reinforcing Steel Including Effect of Buckling. *Journal of Structural Engineering 125(6)*, 605-612.

Sezen, H., & Setzler, E. (2008). Reinforcement Slip in Reinforced Concrete Columns. *ACI Structural Journal 105(3)*, 280-289.

Standards New Zealand. (2006). *Concrete Structures Standard SNZ (3101-2006)*. Wellington, New Zealand.

Su, R., & Wong, S. (2007). Seismic behavior of slender reinforced concrete shear walls under high axial load ratio. *Engineering Structures 29*, 1957-1965.

Takahashi, S., Yoshida, K., Ichinose, T., Sanada, Y., Matsumoto, K., Fukuyama, H., et al. (2013). Flexural Drift Capacity of Reinforced Concrete Wall with Limited Confinement. *ACI Structural Journal 110(1)*, 95-104.

Uniform Building Code (UBC-97). (1997). *Uniform Building Code.* International Conference of Building Officials. Whittier, California.

Wallace, J., Massone, L., Bonelli, P., Dragovich, J., Lagos, R., Lüders, C., et al. (2012). Damage and Implications for Seismic Design of RC Structural Wall Buildings. *Earthquake Spectra 28(S1)*, S281-S299.

Westenenk, B., De la Llera, J., Besa, J., Jünemann, R., Moehle, J., Lüders, C., et al. (2012). Response of Reinforced Concrete Buildings in Concepción During the Maule Earthquake. *Earthquake Sprectra 28(S1)*, S257-S280.

Wood, S. L. (1991). Performance of Reinforced Concrete Buildings During the 1985 Chile Earthquake: Implications for the Design of Structural Walls. *Earthquake Spectra 7(4)*, 607-638.

Wood, S. L., Wight, J. K., & Moehle, J. P. (1987). The 1985 Chile Earthquake: Observations on Earthquake-Resistant Construction in Viña del Mar. *Civil Engineering Studies, Structural Research Series No. 532, Univeristy of Illinois, Urbana*.

Zhang, Y., & Wang, Z. (2000). Seismic Behavior of Reinforced Concrete Shear Walls Subjected to High Axial Loading. *ACI Structural Journal 97(5)*, 739-750.

A P P E N D I C E S

APPENDIX A. MATERIAL TESTING

A.1 Concrete

The concrete used in the construction of the walls and top beams was pre-mixed with a specified characteristic strength of 20 MPa and maximum aggregate size of 11 mm. The concrete of the bottom bases was cast at the construction site using a mixer following the dosification in Table A.1. Standard cylindrical samples (10 cm diameter x 20 cm high and 15 cm diameter x 30 cm high) were cast during construction. The wall specimens and the cylinders were cured with plastic for 7 days.

The cylinders were tested in compression in order to obtain the concrete strength of the wall specimens. The average concrete strength after 56 days for the wall base beams was 21.1 MPa. The concrete used for the walls and the top beams was tested after 7 and 28 days and at the day of the first experimental test. The measured strengths of this concrete are shown in Table A.2

Table A.1. Concrete dosification for the wall base beams

Material	**Saturated Surface Dry Weight (kg)**	**(lbf)**
Cement (Melón especial and Bíobío especial)	392	178
Gravel (10 mm max size)	995	452
Sand	802	365
Water	204	93
Total for 1 m^3 of concrete	**2393**	**1088**

Figure A.1. Concrete samples and compressive test

Table A.2. Measured concrete strength for wall specimens

Cylinder	Age (days)	fc' (MPa)	Cylinder	Age (days)	fc' (MPa)
1	7	12.8	7	260	26.7
2	7	15.6	8	260	26.1
3	7	15.0	9	260	27.7
4	28	22.9	10	260	28.9
5	28	23.8	11	260	27.5
6	28	25.5			

A.2 Reinforcing Steel

For the three walls tested in this project, ϕ8 mm and ϕ10 mm A630-420H steel bars were used for vertical reinforcement and ϕ5 mm AT560-500H steel bars were used for horizontal reinforcement. Three bars were tested for each diameter, measuring strength and deformation between the supports of the testing machine. A displacement transducer was also used to measure the steel bar deformation for the ϕ8 mm and ϕ10 mm bars. For the ϕ 5 mm bars, the displacement transducer was installed in only one of the three bars. The testing machine and the displacement transducer are shown in Figure A.2. An offset strain of 0.002 and the initial slope of the stress-strain curve were used to obtain the yield strength. The final length of each bar was also measured in order to obtain its ultimate strain. The steel properties measured for ϕ5, ϕ8 and ϕ10 bars are summarized in Table A.3, Table A.4 and Table A.5 respectively. Stress-strain curves obtained by the testing machine and the displacement transducer were adjusted in order to obtain realistic data. A Young's modulus of elasticity of 205,000 MPa was supposed to obtain the stress-strain curves shown in Figure A.3, Figure A.4 and Figure A.5.

Figure A.2 Test setup for steel bars

Table A.3. ϕ5 AT560-500H steel bar properties

Bar Specimen	**ϕ5-1**	**ϕ5-2**	**ϕ5-3**	**Average**
Yield strength (Mpa)	607.0	600.3	619.5	608.9
Ultimate strength (Mpa)	677.0	661.5	664.5	667.6
Yield strain	-	-	0.0004	-
Hardening strain	-	-	-	-
Ultimate strain	0.0055	0.0059	0.0055	0.0056
Hardening modulus (Mpa)	-	-	-	-

Table A.4. ϕ8 A630-420H steel bar properties

Bar Specimen	**ϕ8-1**	**ϕ8-2**	**ϕ8-3**	**Average**
Yield strength (MPa)	441.5	460.6	434.8	445.7
Ultimate strength (MPa)	593.7	618.4	584.7	598.9
Yield strain	0.0002	0.0002	0.0002	0.0002
Hardening strain	0.0011	0.0015	0.0015	0.0014
Ultimate strain	0.0173	0.0144	0.0128	0.0148
Hardening modulus (MPa)	4140.3	4144.1	4116.0	4133.5

Table A.5. ϕ10 A630-420H steel bar properties

Bar Specimen	**ϕ10-1**	**ϕ10-2**	**ϕ10-3**	**Average**
Yield strength (MPa)	451.1	438.2	518.3	469.2
Ultimate strength (MPa)	636.8	719.7	670.6	675.7
Yield strain	0.0004	0.0004	0.0003	0.0003
Hardening strain	0.0013	0.0007	0.0021	0.0014
Ultimate strain	0.0169	0.0160	0.0159	0.0162
Hardening modulus (MPa)	4790.5	6941.4	4560.9	5430.9

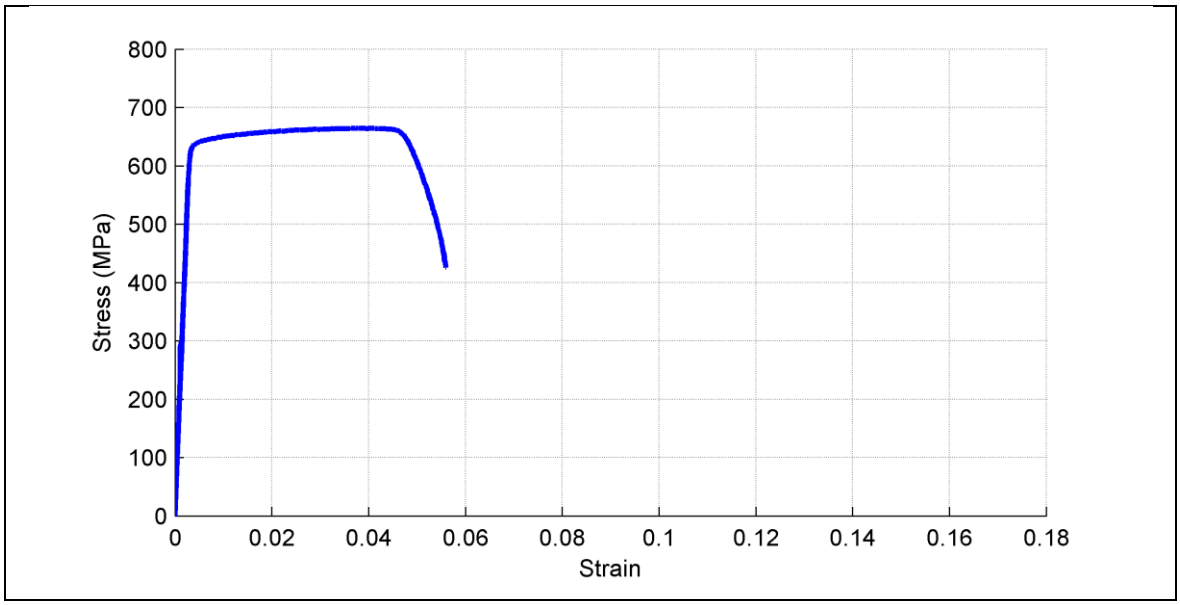

Figure A.3. Stress-strain relationship for ϕ5 AT560-500H steel bar

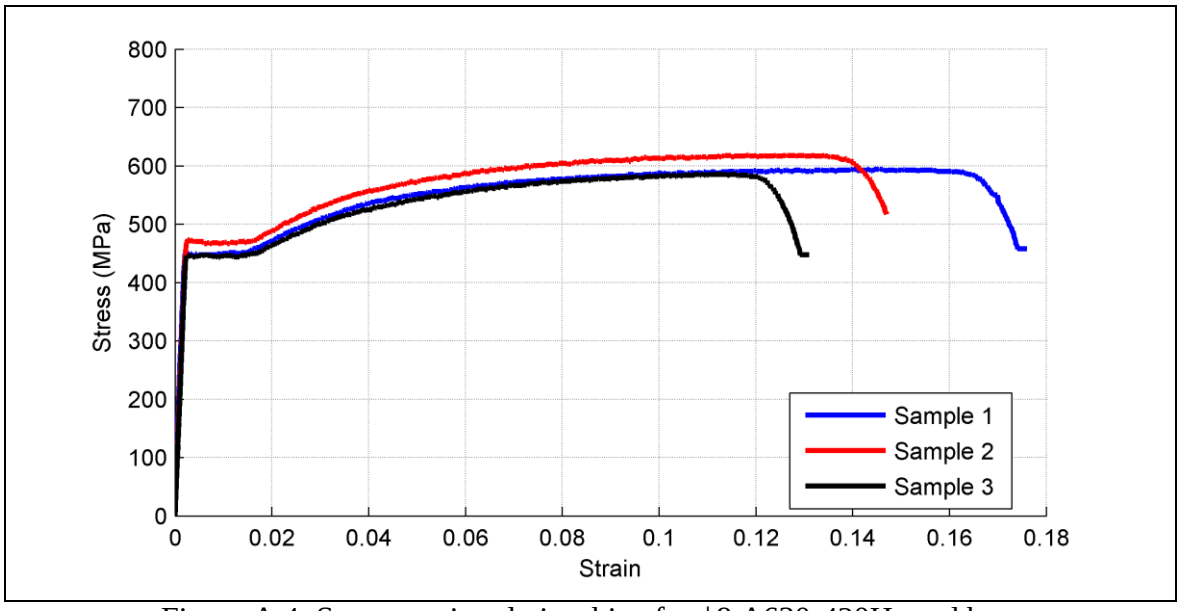

Figure A.4. Stress-strain relationships for ϕ8 A630-420H steel bars

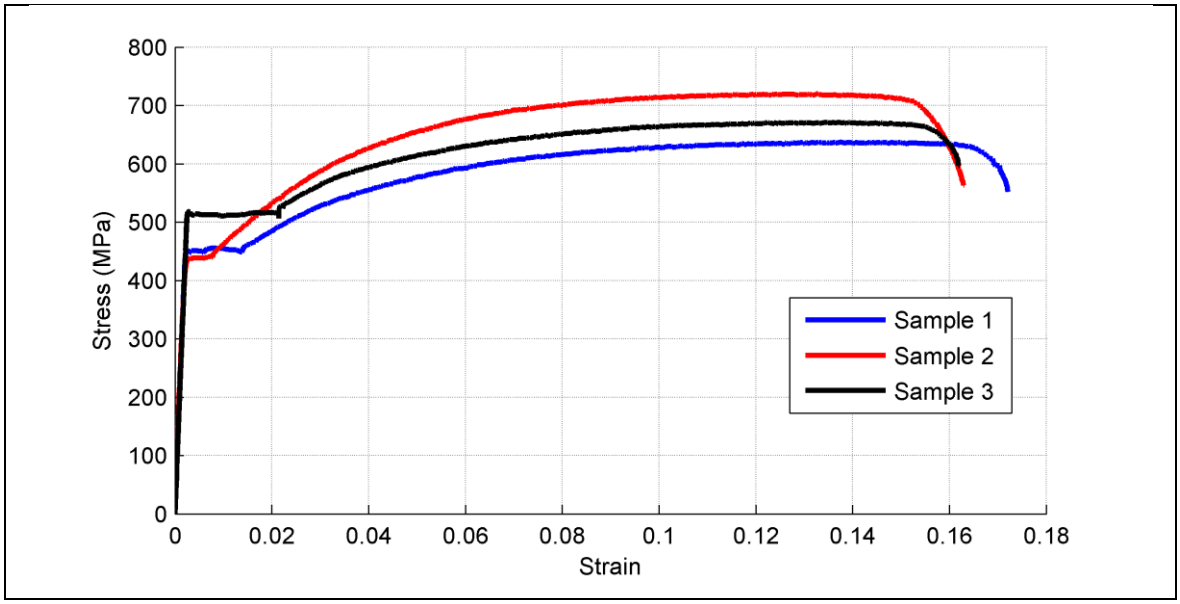

Figure A.5**.** Stress-strain relationships for ϕ10 A630-420H steel bars